USGS
science for a changing world

Prepared in cooperation with the National Park Service

Transient Electromagnetic Soundings in the San Luis Valley, Colorado, near the Great Sand Dunes National Park and Preserve and the Alamosa National Wildlife Refuge (Field Seasons 2007, 2009, and 2011)

Data Series 1043

U.S. Department of the Interior
U.S. Geological Survey

Cover: The Great Sand Dunes (tan feature) viewed from the west with the Sangre de Cristo Mountains in the background. Medano Pass is in the center of the horizon, framed by Mount Herard on the left and Mount Zwischen on the right. The fence line trends east-west and marks the boundary between the historic Baca and Medano Ranches. Rubber rabbitbrush (*Ericameria nauseosa* var. *nauseosa*) and blowout grass (*Redfieldia flexuosa*) or Indian ricegrass (*Achnatherum hymenoides*) cover the area. Photograph by David V. Fitterman, July 16, 2009.

Transient Electromagnetic Soundings in the San Luis Valley, Colorado, near the Great Sand Dunes National Park and Preserve and the Alamosa National Wildlife Refuge (Field Seasons 2007, 2009, and 2011)

By David V. Fitterman

Prepared in cooperation with the National Park Service

Data Series 1043

U.S. Department of the Interior
U.S. Geological Survey

U.S. Department of the Interior
RYAN K. ZINKE, Secretary

U.S. Geological Survey
William H. Werkheiser, Acting Director

U.S. Geological Survey, Reston, Virginia: 2017

Suggested citation:
Fitterman, D.V., 2017, Transient electromagnetic soundings in the San Luis Valley, Colorado, near the Great Sand Dunes National Park and Preserve and the Alamosa National Wildlife Refuge (field seasons 2007, 2009, and 2011): U.S. Geological Survey Data Series 1043, 39 p., https://doi.org/10.3133/ds1043.

ISSN 2327-638X (online)

Contents

Figures

Appendix Figures

Tables

Appendix Tables

Conversion Factors

SI to Inch/Pound

Multiply	By	To obtain
	Length	
meter (m)	3.281	foot (ft)
kilometer (km)	0.6214	mile (mi)
kilometer (km)	0.5400	mile, nautical (nmi)
meter (m)	1.094	yard (yd)
	Area	
square meter (m^2)	10.76	square foot (ft^2)

U.S. customary units to International System of Units

Multiply	By	To obtain
	Length	
foot (ft)	0.3048	meter (m)

Electrical Conductivity and Electrical Resistivity

Multiply	By	To obtain
Electrical conductivity		
siemens per meter (S/m)	1,000	millisiemens per meter (mS/m)
siemens per meter (S/m)	10,000	microsiemens per centimeter (µS/cm)

Electrical conductivity (σ) can be converted to electrical resistivity (ρ) in ohm-meters (ohm-m) as follows.

Electrical conductivity (σ) units	Conversion equation
siemens per meter (S/m)	$\rho = 1/\sigma$
millisiemens per meter (mS/m)	$\rho = 1{,}000/\sigma$
microsiemens per centimeter (µS/cm)	$\rho = 10{,}000/\sigma$

Electrical resistivity (ρ) in ohm-meters (ohm-m) can be converted to electrical conductivity (σ) as follows.

Electrical conductivity (σ) units	Conversion equation
siemens per meter (S/m)	$\sigma = 1/\rho$
millisiemens per meter (mS/m)	$\sigma = 1{,}000/\rho$
microsiemens per centimeter (µS/cm)	$\sigma = 10{,}000/\rho$

Supplemental Information

Specific conductance (SC) refers to fluid electrical conductivity corrected to a temperature of 25 °C. The units of specific conductance are usually in microsiemens per centimeter (µS/cm). The above conversions apply.

Datum

Horizontal coordinate information is referenced to the North American Datum of 1927 (NAD27).

Elevation information is referenced to the National Geodetic Vertical Datum of 1929 (NGVD 29).

Abbreviations

BP	boundary piezometer
CGG	Crustal Geophysics and Geochemistry Science Center
GPS	Global Positioning System
GRSA	Great Sand Dunes National Park and Preserve
NAD27	North American Datum of 1927
NGVD 29	National Geodetic Vertical Datum of 1929
RMS	root mean square
TEM	transient electromagnetic
USGS	U.S. Geological Survey
UTM	Universal Transverse Mercator

Units of Measure

µs	microsecond
µV	microvolt
A	ampere
ft	feet
H	henry
Hz	hertz
ka	kilo-annum
km	kilometer
m	meter
m^2	square meter
Ma	mega-annum
ms	millisecond
mV	millivolt
nV	nanovolt
ohm-m	ohm-meter
s	second
Wb	weber

Data and Software Notation

BP	boundary piezometer sites
GSD	Great Sand Dunes sites
GTF	Geonics TEM File format
HDR	header record (GTF format)
NWR	National Wildlife Refuge sites
OPR	data record (GTF format)
RX	receiver
TX	transmitter

Transient Electromagnetic Soundings in the San Luis Valley, Colorado, near the Great Sand Dunes National Park and Preserve and the Alamosa National Wildlife Preserve Refuge (Field Seasons 2007, 2009, and 2011)

By David V. Fitterman[1]

Abstract

Transient electromagnetic (TEM) soundings were made in the San Luis Valley, Colorado, to map the location of a blue clay unit as well as to investigate the presence of suspected faults. A total of 147 soundings were made near and in Great Sand Dunes National Park and Preserve, and an additional 6 soundings were made near Hansen Bluff on the eastern edge of the Alamosa National Wildlife Refuge. The blue clay is a significant hydrologic feature in the area that separates an unconfined surface aquifer from a deeper confined aquifer. Knowledge of its location is important to regional hydrological models. Previous analysis of well logs has shown that the blue clay has a resistivity of 10 ohm-meters or less, which is in contrast to the higher resistivity of sand, gravel, and other clay units found in the area, making it a very good target for TEM soundings. The top of the blue clay was found to have considerable relief, suggesting the possibility of deformation of the clay during or after deposition. Because of rift activity, deformation is to be expected. Of the TEM profiles made across faults identified by aeromagnetic data, some showed resistivity variations and (or) subsurface elevation relief of resistivity units, suggestive of faulting. Such patterns were not associated with all suspected faults. The Hansen Bluff profile showed variations in resistivity and depth to conductor that coincide with a scarp between the highlands to the east and the floodplain of the Rio Grande to the west.

Introduction

The U.S. Geological Survey (USGS) has been conducting electromagnetic geophysical surveys for several years in the San Luis Valley, Colorado, to obtain subsurface information relevant to understanding geologic deposits associated with an ancient lake that covered much of the San Luis Valley and their influence on the hydrology of the valley. This report describes the results of transient electromagnetic (TEM) soundings that were made in the San Luis Valley to delineate near-surface aquifers and aquitards. This work was funded in part by the National Cooperative Geologic Mapping Program and was done in cooperation with the National Park Service.

The San Luis Valley, located in south-central Colorado, is a relatively flat physiographic feature at the north end of the Rio Grande rift (see fig. 1). It is bounded on the east by the Sangre de Cristo Mountains and on the west by the San Juan Mountains. About 3.7-mega-annum (Ma) basalt flows coming from the south flowed around the eastern and western margins of the San Luis Hills, blocking surface-water drainage from the valley (Machette and others, 2013). Rivers and streams that entered the valley upstream of the dam formed a large lake that covered most of the valley (Siebenthal, 1910). The former body of water is commonly referred to as Lake Alamosa (Machette, 2004; Machette and others, 2007). Fluvio-lacustrine deposits filled the valley, creating the Alamosa Formation, which consists of interbedded blue clay and sand and massive blue clay (Siebenthal, 1910; Huntley, 1979). The Alamosa Formation is buried under alluvium and eolian sand. Over time, the average level of Lake Alamosa increased until around 430 kilo-annum (ka) when the lake overflowed through the San Luis Hills, cutting a drainage channel that is the present course of the Rio Grande (Machette and others, 2013).

A significant component of the Alamosa Formation is a thick, bluish-colored clay called the blue clay (Siebenthal, 1910). The impermeable blue clay separates a near-surface unconfined aquifer from an underlying confined aquifer. Historic and recent drilling results have found that there are numerous clay units shallower than the blue clay that also act as confining units (Grauch and others, 2015) and are part of the transitional, interbedded units described by Siebenthal (1910). Mapping the location of the blue clay gives a regional indication of where the underlying confined aquifer is located. Though the location of the blue clay is important for the development of regional hydrologic models of the San Luis Valley, the transitional zone above the blue clay can significantly influence groundwater flow as well.

[1]U.S. Geological Survey, emeritus

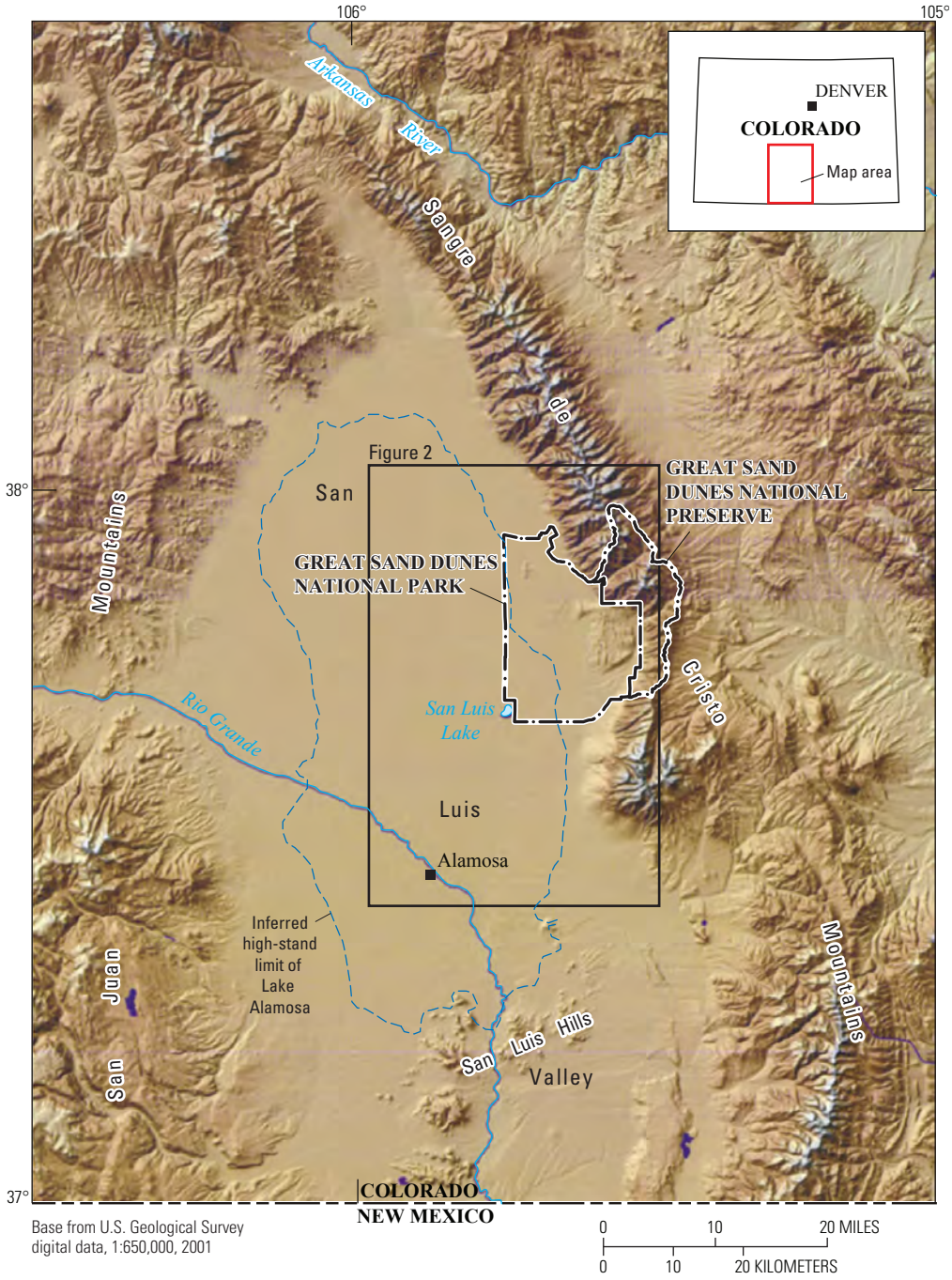

Figure 1. Map of the San Luis Valley, Colorado, and Great Sand Dunes National Park and Preserve. The inferred high-stand limit of Lake Alamosa is from Machette and others (2013). The inset box indicates the overall study area, shown in figure 2.

Because of its low electrical resistivity, the blue clay is an excellent target for TEM soundings (Fitterman and Grauch, 2010). Furthermore, the resistivities of the blue clay, the transitional sand-clay units, and the overlying alluvial sand and gravel and eolian sands are so different that these units can be mapped geophysically. In addition to the blue clay, profiles of TEM soundings were made across known and suspected faults to see if the faults had electrical signatures that could be used to map them. An aeromagnetic survey of the eastern edge of the San Luis Valley detected covered faults that often parallel mapped surface faults (Grauch and others, 2010, 2013). Several of these faults were investigated, and those results are reported herein.

Additionally, a profile was made across Hansen Bluff on the eastern edge of the Alamosa National Wildlife Refuge at the location of an aeromagnetically identified fault parallel to and west of the bluff (V.J.S. Grauch, U.S. Geological Survey, personal commun., 2011) to investigate a possible relation between the fault and the origin of the bluff.

History of Field Effort

The use of TEM soundings to map the blue clay in the San Luis Valley was first reported by Fitterman and de Souza Filho (2009). A small survey of 17 soundings made in 2006 (see fig. 2) was able to map a conductor with a resistivity of 10 ohm-meters (ohm-m) or less. Analysis of cuttings and induction logs from previously drilled wells demonstrated that the conductor corresponded to the blue clay (Fitterman and Grauch, 2010). Based on the success of this work, additional TEM surveys were carried out in subsequent years to better understand the characteristics and extent of the blue clay.

An initial TEM survey was made in the area in 2006 to assess the applicability of the TEM method for mapping clay units (Fitterman and de Souza Filho, 2009). A summary of the follow-on field work carried out from 2007 through 2011 is given below.

Field Season Summary 2007

The goal of the 2007 field work was to increase the TEM coverage from the previous field season (Fitterman and de Souza Filho, 2009) to better define the location and characteristics of the blue clay. Detailed profiles were made along drainages running from the base of the Sangre de Cristo Mountains on the eastern edge of the valley towards the valley floor. The drainages followed include, in order from north to south, Deadman Creek, Short Creek towards Antelope Springs, Sand Creek to Arena Creek, Big Spring Creek, and Little Spring Creek (see fig. 2). Soundings were made in Great Sand Dunes National Park and Preserve (GRSA), which includes portions of the Mendano-Zapata Ranch managed by the Nature Conservancy, and the Baca National Wildlife Refuge managed by the U.S. Fish and Wildlife Service. A total of 44 TEM soundings were made along five profiles. All profiles are oriented roughly perpendicular to the mountain front.

A Geonics Limited PROTEM-D receiver was used with a battery-powered Geonics Limited EM-47 transmitter. A square transmitter loop with a nominal side length of 38.1 meters (m) was used. A single-component receiver coil with a moment of 31.4 square meters (m^2) was placed at the center of the transmitter loop. A perceived intermittent problem developed in the USGS Crustal Geophysics and Geochemistry Science Center (USGS-CGG) PROTEM-D receiver, requiring a switch to a loaner PROTEM-D provided by Geonics Limited. Soundings GSD101 through GSD117 were made with the USGS-CGG PROTEM-D receiver. Analysis of data from soundings GSD101 through GSD117 found that there was no problem with them. Accordingly, they were retained and used. Soundings GSD118 through GSD120 were made with the borrowed PROTEM-D receiver. A second receiver borrowed from USGS New England Water Science Center (an analog PROTEM receiver) was used for soundings GSD121 through GSD144.

Field Season Summary 2009

In 2009, the field work continued with three goals: (1) to provide detailed subsurface information for monitoring wells that were to be drilled for the National Park Service along the western boundary of the GRSA, (2) to continue mapping of the blue clay inside the GRSA and westward into the Baca National Wildlife Refuge, and (3) to make short profiles across suspected faults identified by aeromagnetic surveys along the eastern edge of the valley (fig. 2) (Grauch and others, 2010). A total of 64 soundings were made, including 10 at the boundary piezometer (BP) sites, 47 across suspected faults, and 17 for clay mapping.

All soundings (BP01 through BP10 and GSD201 through GSD254) were made using the USGS-CGG PROTEM-D receiver and the battery-powered EM-47 transmitter. A square transmitter loop with a nominal side length of 38.1 m was used. A single-component receiver coil with a moment of 31.4 m^2 was placed at the center of the transmitter loop.

Field Season Summary 2011

The 2011 field season produced 45 additional soundings, of which 22 were for clay mapping, 17 were across suspected faults, and 6 were near Hansen Bluff in the Alamosa National Wildlife Refuge for the purpose of investigating the origin of the bluff (Valdez, 2007) and its possible relation to a fault parallel to and west of the bluff that was detected in aeromagnetic data.

Soundings GSD301 through GSD339 were made using a Geonics Limited EM-57 MK-2 transmitter attached to a square loop with a side length of 50 m. For these soundings, the receiver coil was a single-component 200-m^2 induction loop located at the center of the transmitter loop. The six soundings made at Hansen Bluff near the Alamosa National Wildlife

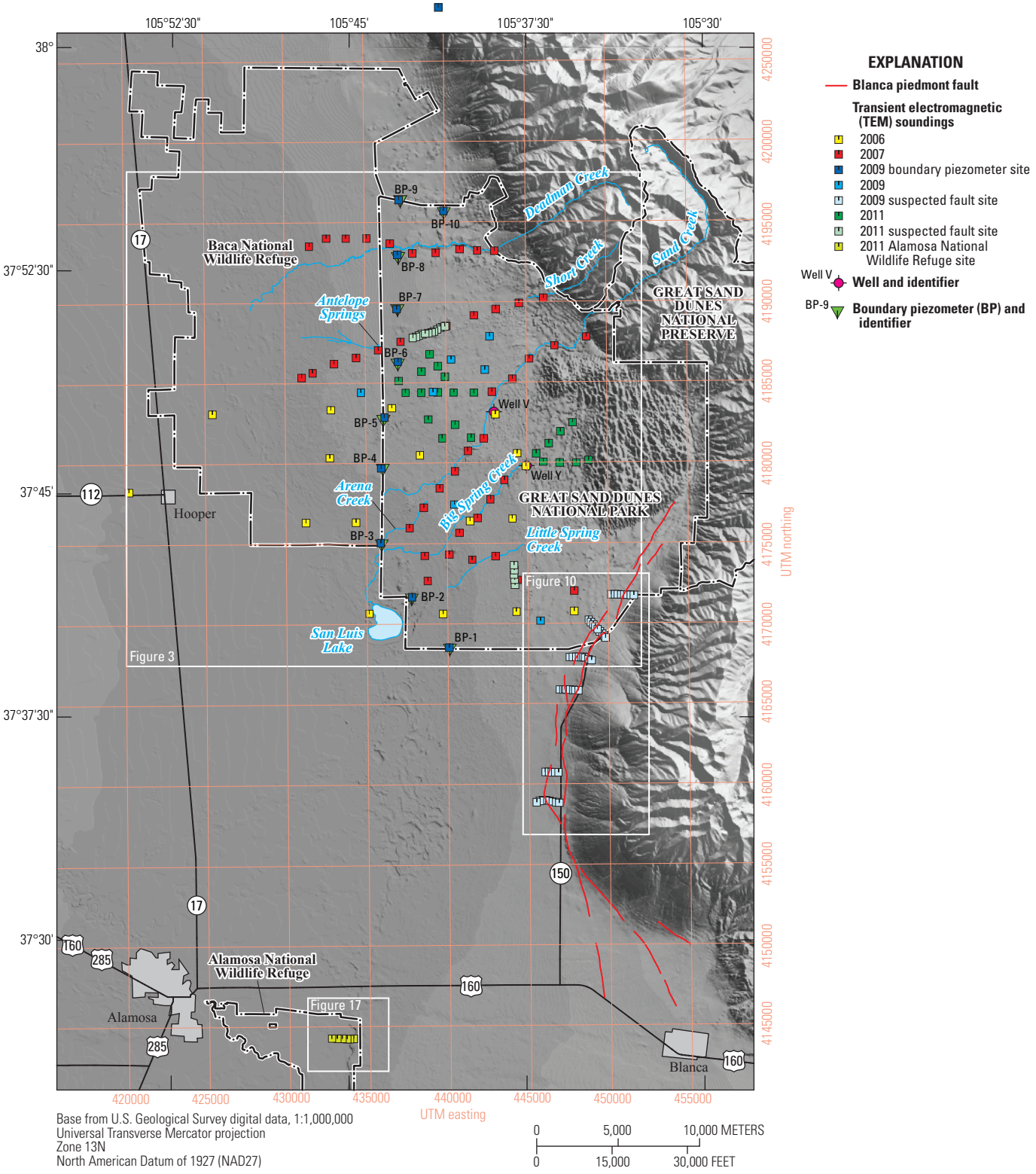

Figure 2. Transient electromagnetic (TEM) sounding location map. Inset boxes show the locations of the three study areas: the area of the blue clay investigation (figure 3); the profiles across the Blanca piedmont fault zone (figure 10); and the Hansen Bluff profile location (figure 17). (UTM, Universal Transverse Mercator, in meters)

Refuge (NWR01 through NWR06) used the EM-57 configuration previously mentioned. In addition, a second configuration was used consisting of an EM-47 transmitter attached to the same square loop used for the EM-57 measurements. The receiver coil was replaced with one having a moment of 31.4 m^2. The Hansen Bluff data required special processing because of discrepancies between the EM-47 and EM-57 data (see appendix 1).

Sounding Locations and Elevations

Coordinates of the soundings were determined by Global Positioning System (GPS) measurements and are given in tables 1, 2, and 3 for field seasons 2007, 2009, and 2011, respectively. Horizontal positions are referenced to the North American Datum of 1927 (NAD27). The GPS unit reported positioning error uncertainties of between 4 and 9 m. Most elevations were obtained by using the GPS coordinates to locate the soundings on 7.5-minute topographic maps and then interpolating between the elevation contours. Accuracy is therefore a fraction of the map contour interval. For a few of the 2011 sites that were located on the western portion of the sand dunes where the validity of the contours on the topographic maps is less reliable (GSD327–GSD334), high-resolution GPS measurements were used to determine elevations. These elevations were far better than those obtained from the topographic maps. The vertical reference for all elevations is the National Geodetic Vertical Datum of 1929 (NGVD 29).

Description of Transient Electromagnetic Sounding

The TEM method was originally developed for use in mineral exploration (Kaufman and Keller, 1983; McNeill, 1990), but over the past 25 years its use has expanded to groundwater and environmental investigations (Fitterman and Stewart, 1986; Fitterman, 1989; Goldman and others, 1991; Fitterman and others, 1999; Fitterman and Labson, 2005).

Soundings are made by passing a current through a large, square transmitter loop. The current flow generates a steady magnetic field. Abruptly shutting off the current flow disrupts the magnetic field and induces a circulating current system in the ground below the transmitter loop. The diffusion of these induced currents is controlled by the electrical conductivity of the ground. The current attenuation is small in conductive regions, and the current passes slowly through them. Resistive regions (with low conductivity), on the other hand, attenuate the current flow. Current traverses these regions more rapidly than in conductive regions. The circulating induced currents produce a secondary magnetic field that is sensed by a receiver coil located at the center of the transmitter loop. Because of the relationship of the electrical conductivity structure of the ground, the current diffusion, and the secondary magnetic field, the voltage recorded by the receiver can be used to estimate the ground conductivity. The result is that the measured voltage-time curves, or transients, can be converted into resistivity-depth functions by a nonlinear parameter estimation process called inversion (Hohmann and Raiche, 1988; Fitterman and Labson, 2005; Oldenburg and Li, 2005).

The equipment used for the various field seasons was described above. Two transmitters were used for the measurements: a battery-powered Geonics Limited EM-47 transmitter and a generator-powered Geonics Limited EM-57 transmitter for deeper exploration. Square transmitter loops were used with nominal side lengths of 38.1 m or 50 m.

For the EM-47 configuration, the transmitter current was typically 2.5 amperes (A). The receiver coil was a rigid loop about 1 m in diameter with a moment of 31.4 m^2. The receiver coil was located at the center of the transmitter loop. After adjusting receiver gain to an appropriate level, measurements were made using base-frequency repetition rates of 285 hertz (Hz) and 30 Hz. The base frequency controls the time range over which the transient is recorded. There are 20 logarithmically spaced measurement gates associated with each base frequency. Each measurement represents a stack of several hundred individual transients. Data processing procedures are discussed in appendix 1.

For the EM-57 configuration, the transmitter current was typically 26 A, and the receiver coil located at the center of the transmitter loop had a moment of 200 m^2. The measurement technique was similar to the EM-47 configuration; however, the base-frequency repetition rates were typically 30 Hz and 3 Hz.

Data Quality and Averaging Procedure

All of the soundings were of very high quality because of the low background noise in the field area and the long integration times used during data recording. Data summaries and plots are described in appendix 4 and can be found in the data release by Fitterman (2016) that accompanies this data series.

Anywhere from 5 to 13 TEM measurements were averaged for each sounding for each base frequency to reduce and estimate measurement error. Averaging was done using the program NTEMAVG[1] for the analog PROTEM receiver data and the program DTEMAVG for the digital PROTEM-D receiver data. Some selective editing of the data was performed manually when it was obvious that a particular datum was significantly different from neighboring points. The average and standard deviation were calculated with the remaining measurements. The standard deviation of the apparent resistivity for the ultra-high (data code: uh, 285 Hz) base frequency was as low as 0.1 percent at early times. For most of the soundings, the noise increased to only 1–3 percent

[1]The programs NTEMAVG and DTEMAVG are unpublished and were developed by D.V. Fitterman, U.S. Geological Survey.

Table 1. Universal Transverse Mercator (UTM) coordinates and elevations of transient electromagnetic (TEM) soundings made in 2007.

Sounding	Easting[1] (meters)	Northing[1] (meters)	Elevation[2] (meters)
Great Sand Dunes National Park and Preserve			
GSD101	443085	4193161	2377.4
GSD102	442016	4193194	2353.1
GSD103	440930	4193282	2347.0
GSD104	439429	4193075	2337.8
GSD105	437976	4193037	2328.7
GSD106	436592	4193665	2325.6
GSD107	435139	4193987	2318.0
GSD108	433847	4193994	2311.6
GSD109	432638	4194004	2307.3
GSD110	431559	4193515	2304.3
GSD111	448758	4187798	2438.4
GSD112	446115	4190223	2462.8
GSD113	444149	4185194	2359.2
GSD114	445197	4186452	2364.0
GSD115	446774	4187266	2395.7
GSD116	442860	4184406	2359.2
GSD117	444585	4189915	2395.7
GSD118	443138	4189554	2368.3
GSD119	441775	4189164	2354.6
GSD120	440054	4188509	2343.9
GSD121	438571	4188017	2331.7
GSD122	437206	4187551	2324.1
GSD123	435812	4187032	2316.5
GSD124	434431	4186571	2311.9
GSD125	433058	4186204	2307.3
GSD126	431726	4185631	2304.3
GSD127	431036	4185341	2302.2
GSD128	442339	4181510	2336.3
GSD129	441342	4180731	2331.7
GSD130	440529	4179471	2321.1
GSD131	439569	4178416	2313.4
GSD132	438580	4177226	2307.3
GSD133	437682	4175958	2299.7
GSD134	443596	4178920	2327.1
GSD135	442719	4177713	2321.1
GSD136	441919	4176555	2313.4
GSD137	440783	4175644	2306.4
GSD138	440143	4174297	2301.2
GSD139	438620	4174222	2298.2
GSD140	438783	4172661	2296.7
GSD141	441562	4173966	2305.8
GSD142	443016	4174182	2314.0
GSD143	444361	4172696	2323.2
GSD144	447892	4171996	2356.1

[1]Coordinates are in the North American Datum of 1927 (NAD27) Universal Transverse Mercator (UTM) zone 13N.

[2]Elevations are in the National Geodetic Vertical Datum of 1929 (NGVD 29) interpolated from 7.5-minute topographic maps using locations determined from the Global Positioning System (GPS).

Table 2. Universal Transverse Mercator (UTM) coordinates and elevations of transient electromagnetic (TEM) soundings made in 2009.

Sounding	Easting[1] (meters)	Northing[1] (meters)	Elevation[2] (meters)
Great Sand Dunes National Park boundary piezometer sites			
BP01	440086	4168507	2299.7
BP02	437800	4171659	2293.6
BP03	435879	4175041	2295.1
BP04	435951	4179684	2308.3
BP05	436171	4182848	2319.5
BP06	437029	4186303	2321.1
BP07	436979	4189587	2325.0
BP08	437052	4192958	2327.1
BP09	437155	4196368	2331.7
BP10	439953	4195643	2350.0
Great Sand Dunes National Park and Preserve			
GSD201	450197	4171749	2386.6
GSD202	450420	4171748	2390.2
GSD203	450598	4171738	2391.5
GSD204	450800	4171735	2392.1
GSD205	451000	4171720	2395.7
GSD206	451198	4171710	2400.6
GSD207	451393	4171697	2406.4
GSD208	451595	4171691	2418.6
GSD209	447572	4167862	2348.5
GSD210	447766	4167873	2351.5
GSD211	447972	4167865	2355.5
GSD212	448142	4167872	2360.7
GSD213	448319	4167853	2366.8
GSD214	448425	4167867	2369.8
GSD215	448528	4167833	2374.4
GSD216	448744	4167726	2379.9
GSD217	448936	4167664	2391.2
GSD218	448773	4170171	2365.2
GSD219	448911	4170025	2368.3
GSD220	449060	4169886	2368.3
GSD221	449187	4169738	2368.3
GSD222	449318	4169588	2365.9
GSD223	449461	4169451	2370.7
GSD224	449616	4169310	2377.4
GSD225	449741	4169154	2383.5
GSD226	449820	4169063	2389.6
GSD227	446958	4165860	2334.8
GSD228	447156	4165848	2333.2
GSD229	447259	4165852	2334.8
GSD230	447358	4165855	2337.8
GSD231	447577	4165835	2343.9
GSD232	447768	4165816	2353.1
GSD233	447910	4165809	2363.7
GSD234	448105	4165800	2371.3
GSD235	446008	4160738	2324.1
GSD236	446221	4160731	2328.7
GSD237	446409	4160703	2330.5
GSD238	446815	4160696	2340.9
GSD239	446605	4160706	2338.4
GSD240	440348	4186426	2338.4
GSD241	442425	4185777	2351.5
GSD242	442744	4187852	2359.2
GSD243	439207	4184417	2334.8
GSD244	434723	4184401	2315.3

Table 2. Universal Transverse Mercator (UTM) coordinates and elevations of transient electromagnetic (TEM) soundings made in 2009.—Continued

Sounding	Easting[1] (meters)	Northing[1] (meters)	Elevation[2] (meters)
Great Sand Dunes National Park and Preserve—Continued			
GSD245	445772	4170141	2337.8
GSD246	440487	4177407	2311.9
GSD247	445839	4158979	2318.6
GSD248	446039	4158976	2321.4
GSD249	446242	4158940	2325.0
GSD250	446443	4158895	2327.1
GSD251	446649	4158848	2331.7
GSD252	445645	4158929	2315.9
GSD253	445449	4158852	2314.7
GSD254	446851	4158805	2345.7

[1]Coordinates are in the North American Datum of 1927 (NAD27) Universal Transverse Mercator (UTM) zone 13N.

[2]Elevations are in the National Geodetic Vertical Datum of 1929 (NGVD 29) interpolated from 7.5-minute topographic maps using locations determined from the Global Positioning System (GPS).

in channel 20. The EM-47 (low-power transmitter) high (hi, 30 Hz) base-frequency data had noise levels of 0.5 percent at channel 1, often increasing to very high levels (more than 25 percent) at the last channels. The percent standard deviation usually increases with time after transmitter turnoff because the signal due to the ground becomes small with respect to the background noise level. By the time the noise level reaches 10 percent in apparent resistivity, the data are usually behaving discontinuously from one channel to the next and are not useable. Another measure of whether or not the data are usable is the magnitude of the signal; signal levels at the coil of greater than 2–3 nanovolts per square meter are usually reliable.

The EM-57 (high-power transmitter) high (HI, 30 Hz) base-frequency data had lower noise than the EM-47 data for the same time range. Standard deviation in the first 15 or more channels was about 0.2 percent with values approaching 1 percent near channel 20. Low (LO, 3 Hz) base-frequency data had standard deviations of 0.2 percent at earlier time channels, increasing to about 5 percent at later time channels. The low-frequency data were not used in the inversions as the high-frequency data gave adequate information for our target.

Inversion of Transient Electromagnetic Measurements

The TEM soundings were individually inverted using the simplest model that fit the data. The major features of most soundings could be adequately described with a four-layer model whose resistivities decrease with depth. After determining a preliminary model for each sounding and comparing the results with nearby soundings, additional layers were sometimes added to the models to improve the fit between the observed and computed apparent resistivities. Layers that were unresolvable because they were too thin, or because their resistivity was not significantly different from adjacent layers, were eliminated from the final model. Most final models have between three and five layers. See Fitterman (2016) for detailed inversion results. Where alternative inversion models were considered, they are also presented in the data release.

Description of Results

The TEM soundings were focused on four geologic targets: the blue clay, suspected faults inside the boundary of ancient Lake Alamosa, suspected faults near the basin margin, and Hansen Bluff to obtain information about its origin. While not on the edge of the basin, Hansen Bluff may be associated with faulting similar to that seen near the eastern edge of the San Luis Valley.

Figure 3 shows the location of the TEM soundings used to map the blue clay. The soundings were situated to provide a broad coverage of the area. In two areas, suspected fault features were investigated using densely spaced lines: the Antelope Springs line and the Little Spring Creek line (marked as AS and LS, respectively, in fig. 3). A special group of soundings, identified with a prefix of BP, were made along the western boundary of the GRSA where monitoring piezometers were installed.

Until these soundings, well information has been the only source of information about the blue clay and other near-surface geologic units in the valley. Exploratory wells drilled for hydrologic investigations provided information on the depth and electrical characteristics of the blue clay (HRS Water Consultants Inc., 1999). Analysis of these data found that the blue clay typically has resistivities of less than 10 ohm-m, while gray clays, which are often found above the blue clay and interbedded with sand, have average resistivities of 20 ohm-m or more (Fitterman and Grauch, 2010). In contrast, the sand has resistivities from 30 to greater than 500 ohm-m. These differences in resistivity are significant enough that the various units can be identified by TEM measurements with reasonable certainty.

Table 3. Universal Transverse Mercator (UTM) coordinates and elevations of transient electromagnetic (TEM) soundings made in 2011.

Sounding	Easting[1] (meters)	Northing[1] (meters)	Elevation[2] (meters)
Great Sand Dunes National Park and Preserve			
GSD301	439801	4188431	2342.1
GSD302	439669	4188399	2341.5
GSD303	439497	4188294	2340.9
GSD304	439290	4188175	2339.3
GSD305	439146	4188126	2337.2
GSD306	438931	4188073	2335.1
GSD307	438738	4188049	2333.5
GSD308	438535	4188010	2332.9
GSD309	438353	4187940	2331.4
GSD310	438165	4187856	2330.5
GSD311	437973	4187782	2329.3
GSD312	439970	4188500	2342.7
GSD313	441744	4184358	2350.0
GSD314	440484	4184372	2343.0
GSD315	439498	4184383	2333.2
GSD316	438473	4184374	2330.2
GSD317	437497	4184374	2326.2
GSD318	437071	4185118	2324.1
GSD319	438893	4182709	2330.2
GSD320	440556	4182367	2334.2
GSD321	441541	4181559	2334.8
GSD322	439760	4181524	2328.4
GSD323	439958	4185352	2339.9
GSD324	439518	4186017	2334.5
GSD325	438495	4185693	2330.2
GSD326	439016	4186761	2334.5
GSD327	445588	4180548	[3]2350.4
GSD328	446368	4181186	[3]2365.1
GSD329	447096	4181920	[3]2378.8
GSD330	447867	4182472	[3]2410.2
GSD331	446028	4180031	[3]2351.4
GSD332	447042	4179971	[3]2362.7
GSD333	448088	4179967	[3]2392.7
GSD334	448840	4180131	[3]2441.6
GSD335	444208	4172391	2322.6
GSD336	444196	4172697	2322.6
GSD337	444151	4173016	2321.7
GSD338	444173	4173298	2321.4
GSD339	444161	4173608	2321.7
Alamosa National Wildlife Refuge			
NWR01	433953	4144231	2300.3
NWR02	433721	4144206	2291.5
NWR03	433549	4144211	2292.1
NWR04	433257	4144230	2292.1
NWR05	432941	4144240	2292.1
NWR06	432603	4144249	2292.1

[1]Coordinates are in the North American Datum of 1927 (NAD27) Universal Transverse Mercator (UTM) zone 13N.

[2]Elevations are in the National Geodetic Vertical Datum of 1929 (NGVD 29) interpolated from 7.5-minute topographic maps using locations determined from the Global Positioning System (GPS).

[3]Elevations for these locations were determined by using high-resolution GPS measurements.

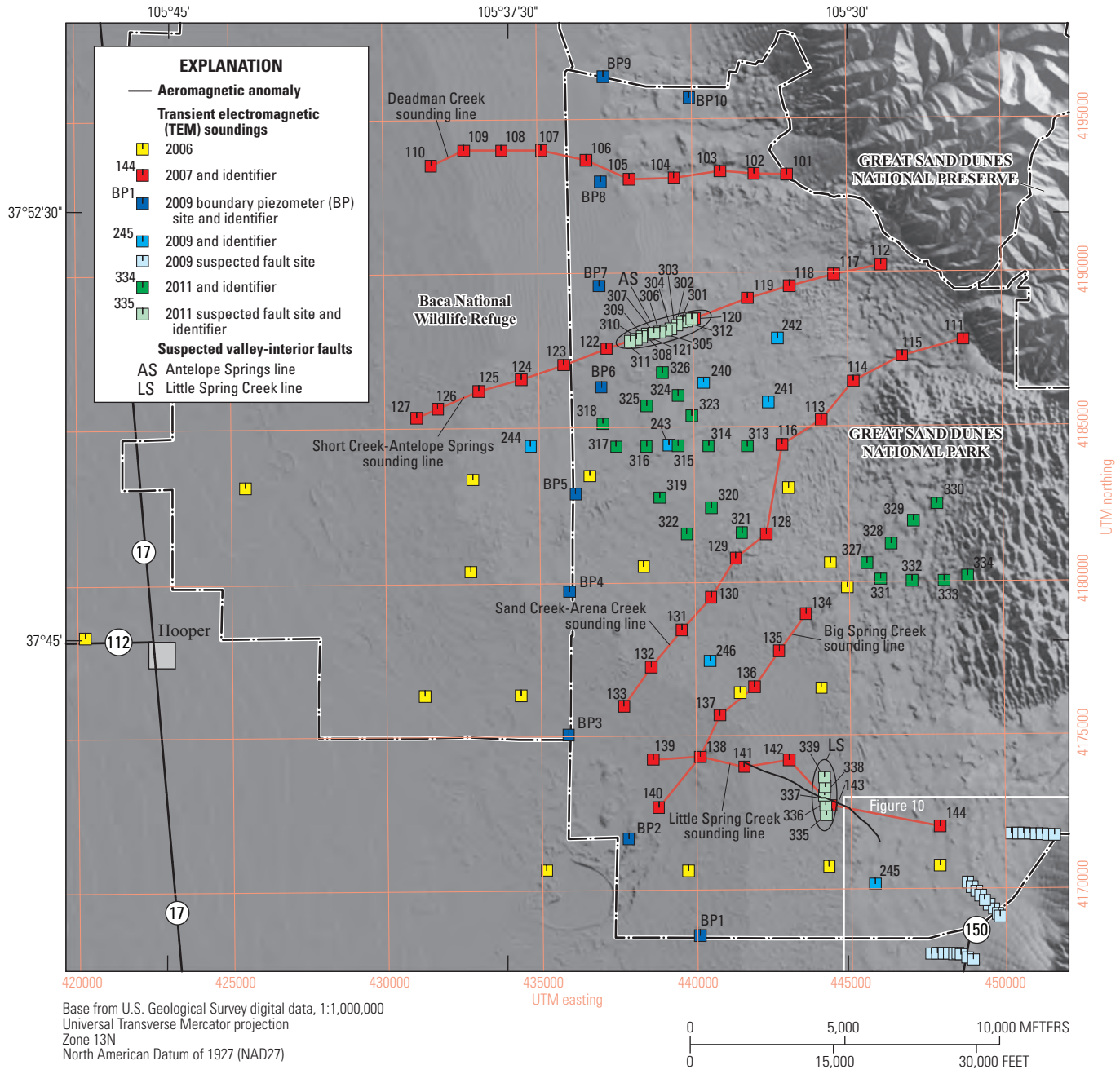

Figure 3. Location map of transient electromagnetic (TEM) soundings made to map depth to the blue clay. For clarity, the prefix GSD was removed from sounding identifiers. The five geophysical transects made in 2007 are indicated by red squares connected by red lines and are named for the drainage areas they roughly follow (see fig. 2). The TEM lines used to investigate suspected valley-interior faults are the Antelope Springs line (AS) and the Little Spring Creek line (LS). The black line crossing through the Little Spring Creek line is an aeromagnetic anomaly that could be caused by a fault or an old river channel (V.J.S. Grauch, U.S. Geological Survey, written commun., 2015). Soundings made at the sites of park boundary piezometers (BP) are shown by dark blue squares. Inset box shows overlap with area shown in figure 10. See figure 2 for location relative to other study areas. (UTM, Universal Transverse Mercator, in meters)

Western GRSA Boundary Piezometers

As part of a court ruling granting an in-place groundwater right, the National Park Service was required to install a set of piezometers along the western boundary of the GRSA to monitor water levels (Colorado District Court Water Division No. 3, 2004). The USGS made a series of TEM soundings for the National Park Service at the proposed drilling sites to estimate the depth to the blue clay for planning of drilling depths and expenses. The results are shown as a cross section in figure 4. The inversion models, which are roughly evenly spaced (average spacing is about 3.6 kilometers [km]), are displayed in the figure as if they formed a straight line. The models are characterized by resistivity values that decrease with depth. The interpreted surface resistivity is very high with values that range from approximately 100 to greater than 1,000 ohm-m. This layer is interpreted to be dry sand. At some locations, the surface layer is underlain by a moderately resistive layer (50–95 ohm-m) interpreted to be a mixture of sand and gravel. The combined thickness of these two layers ranges from less than 10 m to greater than 120 m. As can be seen in the cross section, there is a deepening of the resistive units in the middle of the section beneath stations BP6 and BP7. The next layer is a transitional conductor with resistivities in the range of 12–50 ohm-m. The thickness of the transitional conductor is in the range of 30–100 m with most values between 50 and 60 m. The transitional conductor is interpreted as being a mixture of sand and gray clay. The deepest layer is a conductor whose resistivity is less than 10 ohm-m. The conductor, which was seen at all locations except for station BP10, is interpreted to be the blue clay.

The conductor is deepest near sounding BP7 and becomes shallower to the south. From the deepest point to the shallowest at BP1, the surface of the conductor rises a bit more than 100 m, and its depth decreases from 183 m to 51 m. Notice that the surface elevation drops by more than 30 m between BP7 and BP1. These elevation and depth changes are small compared to the 20-km distance between the soundings.

The USGS drilled well BP-3-USGS adjacent to the National Park Service piezometer well site BP-3 and sounding BP3 for the purposes of obtaining geological samples and geophysical logs (Grauch and others, 2015). Well BP-3-USGS was drilled to a depth of 326 feet (ft) (99.4 m). Grauch and others (2015) generalize the sediments encountered in the well into three lithologic packages: (1) mostly sand from the surface to a depth of 23.5 m (77 ft); (2) interbedded sand, silt, and clay with decreasing grain size with depth in the interval 23.5 to 70.7 m (77 to 232 ft); and (3) alternating layers of massive clay and fine sand to silt from 70.7 to 99.4 m (232 to 326 ft). The topmost clay layer in the third package has a blue tint and was deemed to correlate with the blue clay. Another confining layer was encountered at a depth of 36.3 m (119 ft) in the second package. When this shallower clay unit was penetrated, water began flowing from the well, suggesting that this clay unit at an elevation of 2,260 m above sea level (7,415 ft) marks the top of the confined San Luis Valley aquifer.

Sounding BP3 consists of a thin (4.0 m), very high resistivity (500 ohm-m) surface layer underlain by a high-resistivity (80 ohm-m) layer 21.7 m thick. (This and other soundings can be seen in Fitterman [2016].) The third layer is moderately conductive (29.7 ohm-m) with a thickness of 46.0 m. The conductive (6.7 ohm-m) fourth layer starts at a depth of 71.7 m. Based on earlier well information (Fitterman and Grauch, 2010), these layers are interpreted as dry sand, sand and gravel, a mixture of sand and gray clay, and the blue clay. The inversion depth of the top of the blue clay is in good agreement with the findings of well BP-3-USGS (see Grauch and others, 2015, fig. 12).

After drilling of the National Park Service BP wells was completed, the TEM results were considered a “remarkably accurate” predictor of the sand-to-clay transition in these wells (HRS Water Consultants Inc., 2009); however, most of these wells were not drilled deep enough to reach the blue clay.

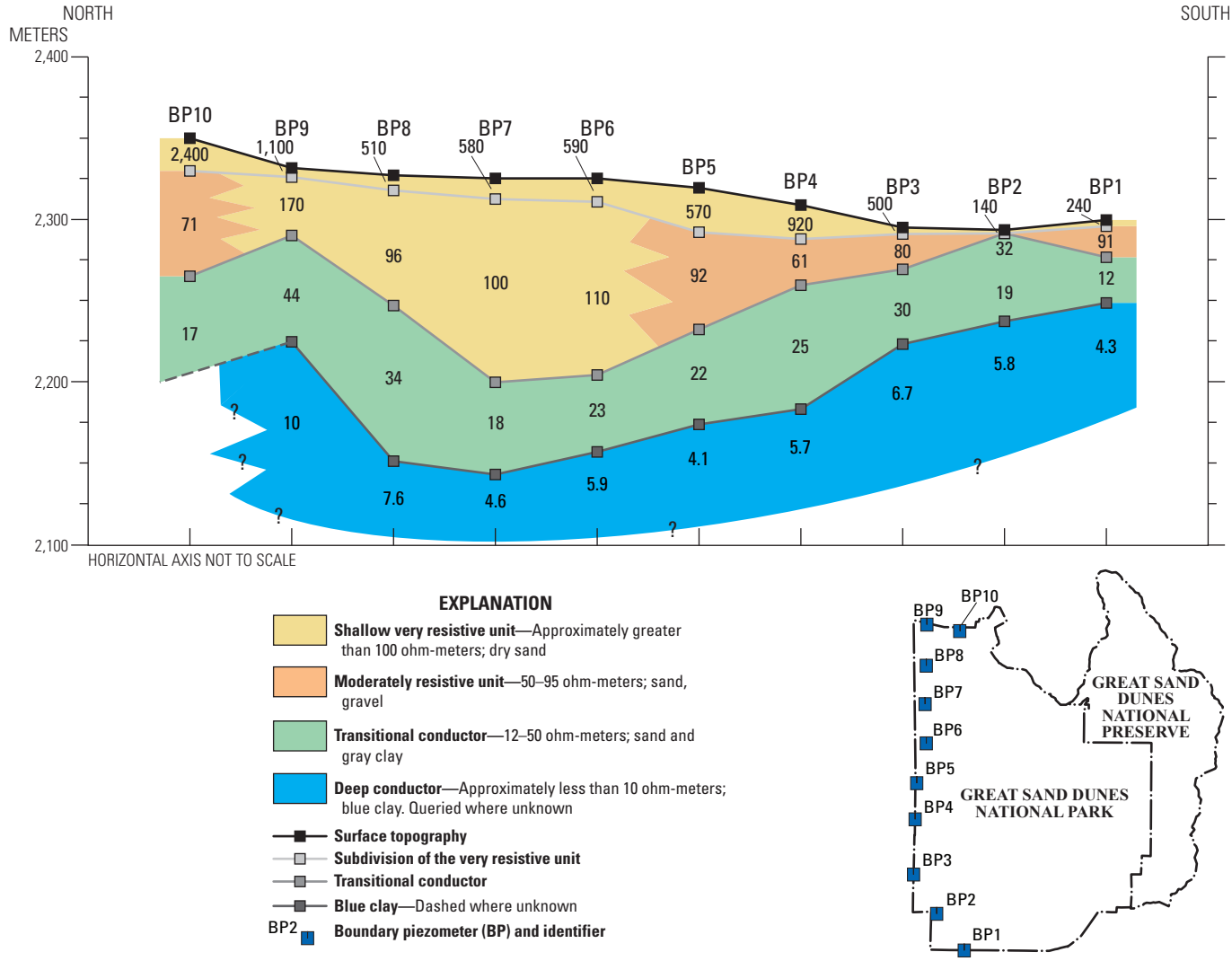

Figure 4. Transient electromagnetic (TEM) cross section of soundings near monitoring piezometer locations along the western boundary of Great Sand Dunes National Park and Preserve.

Mapping the Blue Clay

One of the goals of this field work was to map the geometry of the top of the blue clay. By using the TEM inversion results, a map of the depth of the blue clay was constructed based on a criterion of an interpreted resistivity of less than 10 ohm-m (fig. 5). A total of 107 soundings met this criterion and was used to construct the map. Depths range from 45 m to greater than 180 m. In general, the depth of the blue clay is greater in the northern part of the study area. Sounding density is high enough that most of the features on the map show rather smooth variation with position. Only one point in the northern line of soundings (GSD104) suggests the possibility of a single point anomaly with a depth of a bit less than 140 m. As the topography changes significantly across the area, a map of the elevation of the blue clay gives more insight as to the subsurface geometry of the clay (fig. 6).

The elevation map shows a basinlike feature which is deepest in the northern part of the survey area. When displayed as elevation, the anomalous point associated with GSD104 mentioned above blends in more with the surrounding elevations. There is a regional gradient in the elevation map emanating from the basin and oriented in the southwest direction. This gradient is smooth and fairly constant. Along the east side of the basinlike feature and extending to the south, there is a large, easterly directed gradient that suggests the possibility of an underlying structure. A dense line of soundings (the Antelope Springs line, marked AS in fig. 3) was made across this gradient and is discussed in the next section.

Suspected Valley-Interior Faults

Two profiles were made in the interior of the valley across suspected faults identified in the aeromagnetic data (Grauch and others, 2010). The profiles are named the Antelope Springs line and the Little Springs Creek line (features AS and LS in figure 3) and are discussed below.

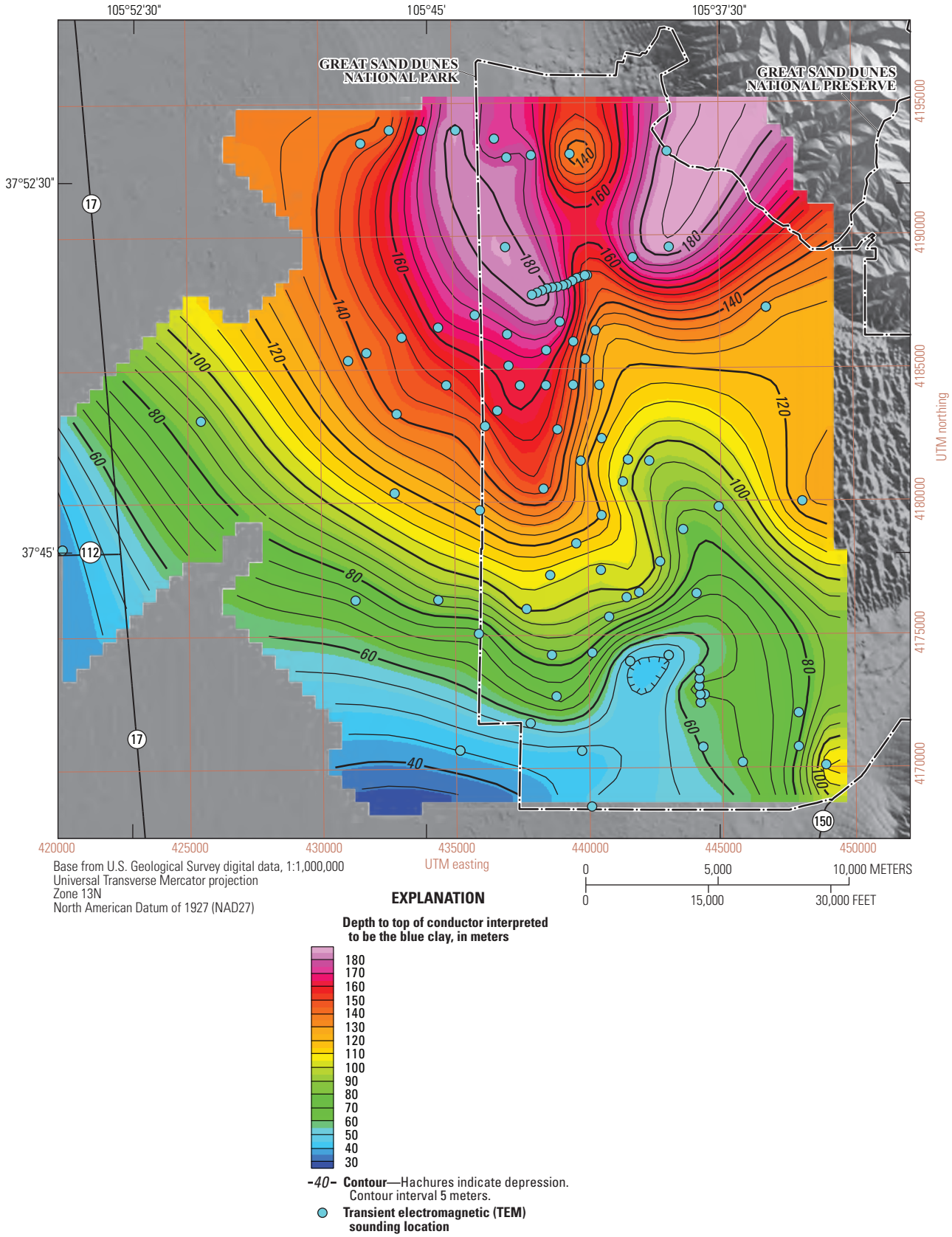

Figure 5. Map of depth to top of conductor intrepreted to be the blue clay. Transient electromagnetic (TEM) sounding locations are shown as blue circles and include some soundings from Fitterman and de Souza Filho (2009). The locations of soundings that did not detect the blue clay are not shown. (UTM, Universal Transverse Mercator, in meters)

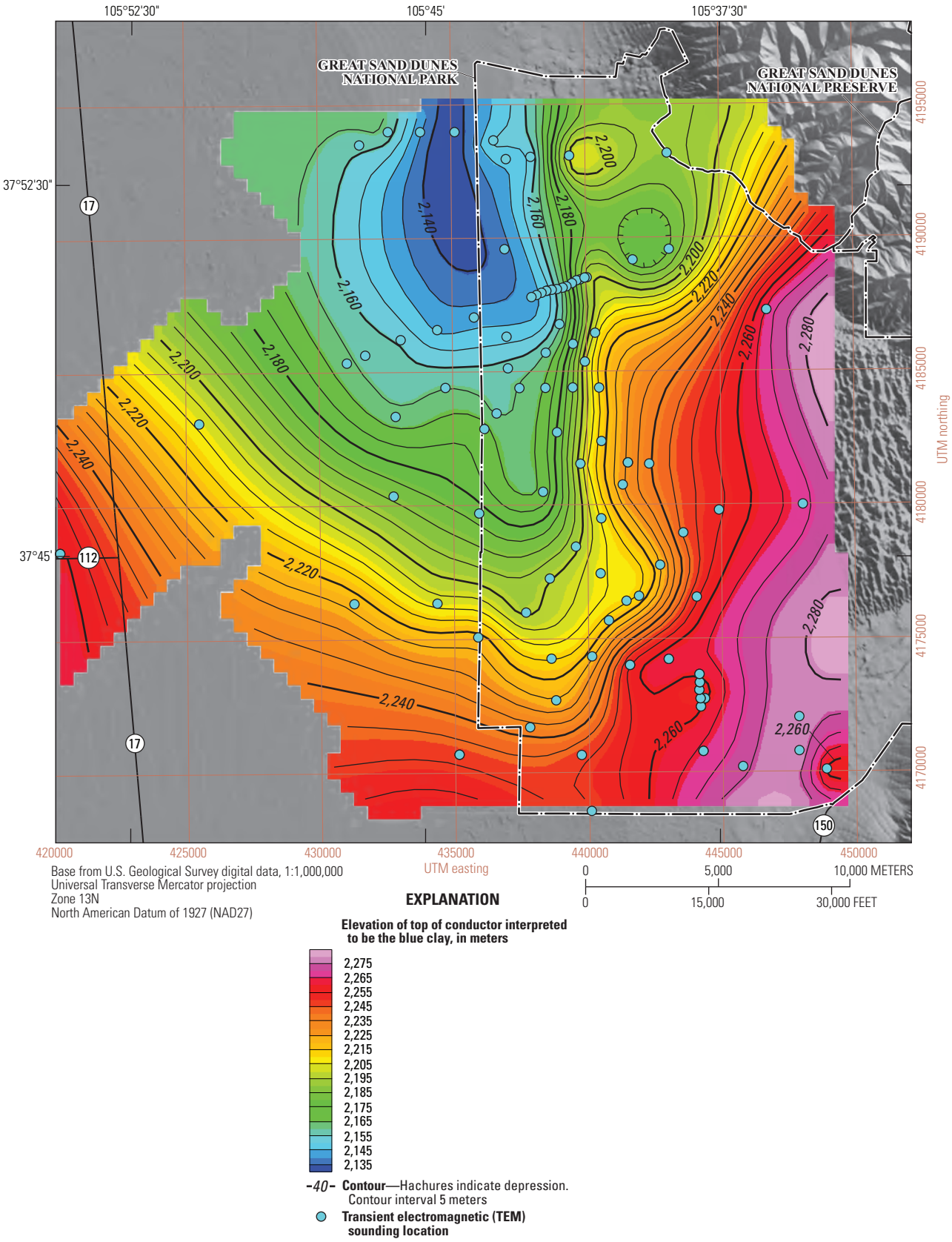

Figure 6. Map of elevation of top of conductor interpreted to be the blue clay. Transient electromagnetic (TEM) sounding locations are shown as blue circles and include some soundings from Fitterman and de Souza Filho (2009). The locations of soundings that did not detect the blue clay are not shown. (UTM, Universal Transverse Mercator, in meters)

Antelope Springs Line

The first soundings made on the Antelope Springs line in 2007 are spaced about 1,400 m apart. A subsequent survey in 2011 over a portion of the original line was made with 200-m intersounding spacing to better resolve the geometry of the blue clay and possible faulting. The resulting cross section is shown in figure 7. (The soundings from 2007 were used to generate the blue clay depth and elevation maps in figures 5 and 6, respectively; however, soundings GSD120 and GSD121 are not shown on the cross section in figure 7.) The soundings are interpreted with three-layer models that have a very resistive (greater than 300 ohm-m) surface layer, a moderately resistive (30–100 ohm-m) second layer, and a conductive (less than 10 ohm-m) third layer. These layers are interpreted to be dry sand, sand and gravel, and the blue clay based on their resistivity ranges. The thickness of the dry sand layer is fairly constant, ranging from 70 to 80 m. The sand and gravel layer thickness ranges between 75 and 100 m, with its thickness decreasing towards the northeast end of the line. The top of the second layer more or less mimics the surface topography, while the top of the third layer does not.

The elevation of the two subsurface interfaces are plotted as a function of distance along the profile in figure 8. The points on the top of the sand and gravel layer are shown in orange, and the points on the top of the blue clay are shown in blue. There is a marked difference in the form of these two interfaces. The first six or seven points on the top of the gravel-sand layer vary in a range of about 10 m. The remainder of the line is characterized by an increase in elevation that flattens out toward the end of the line. The top of the blue clay layer is much more regular and is fit with two straight lines—one going through the first five points, and the other going through the last eight points. The kink in the blue clay surface suggests some sort of deformation around the point where the slope changes (sounding GSD307). The upper interface does not show as regular a behavior, suggesting that different geological processes controlled the shape of each interface.

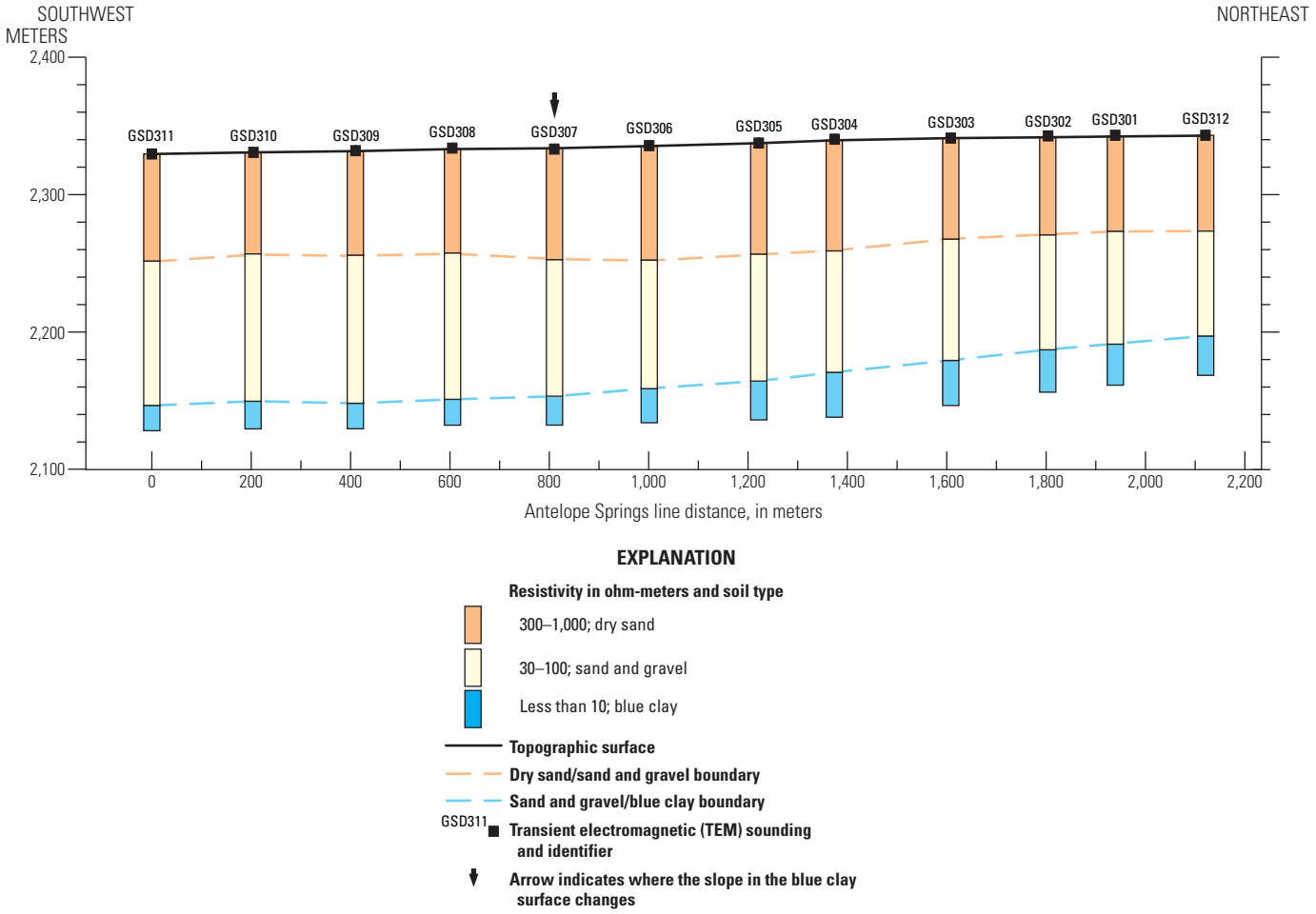

Figure 7. Antelope Springs line transient electromagnetic (TEM) cross section. Three layers are interpreted for each sounding (from surface to depth): dry sand, sand and gravel mixture, and the blue clay. The arrow indicates where the slope in the blue clay surface changes.

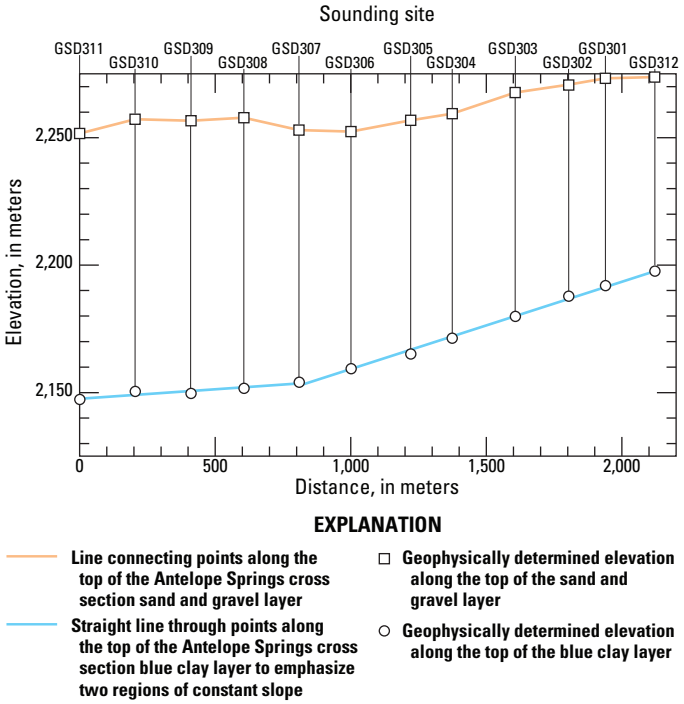

Figure 8. Elevation of the tops of the second and third layers from the Antelope Springs cross section shown in figure 7. The orange line corresponds to the top of the sand and gravel layer. The blue line, corresponding to the top of the blue clay layer, was constructed using two straight lines fit to the data points.

Little Spring Creek Line

Five soundings were made across a suspected fault near Little Spring Creek (see fig. 3). All soundings were interpreted with three-layer models with resistivity decreasing with depth (fig. 9). For all but the most northerly sounding, the surface layer has a resistivity in the range of 100–300 ohm-m. The surface resistivity of sounding GSD339 is higher, at a range of 300–1,000 ohm-m. The high-resistivity surface layer is underlain by a conductive layer (5–10 ohm-m), and the third layer has even lower resistivities (less than 5 ohm-m). The first layer is interpreted to be very dry sand, while the conductive zone below it is considered to be the blue clay. Perhaps decreased water quality is the cause of the very conductive deepest layer.

This location was chosen for study based on a subtle linear aeromagnetic anomaly that could be interpreted as a fault or an old river channel crossing the TEM line at an oblique angle (see fig. 3). Although the TEM results are also ambiguous with regard to the presence of a fault, there is a 10-m depression in the interface between the first and second layers near sounding GSD337. There is also a 20-m depression in the very conductive third layer at sounding GSD338 compared to elevation at soundings GSD336 and GSD339. These depressions could be caused by faulting or a channel, or series of channels, which have crossed the area over time. While the TEM results do not definitively argue for or against the existence of a fault or channels, these data suggest that there is something unusual at this location.

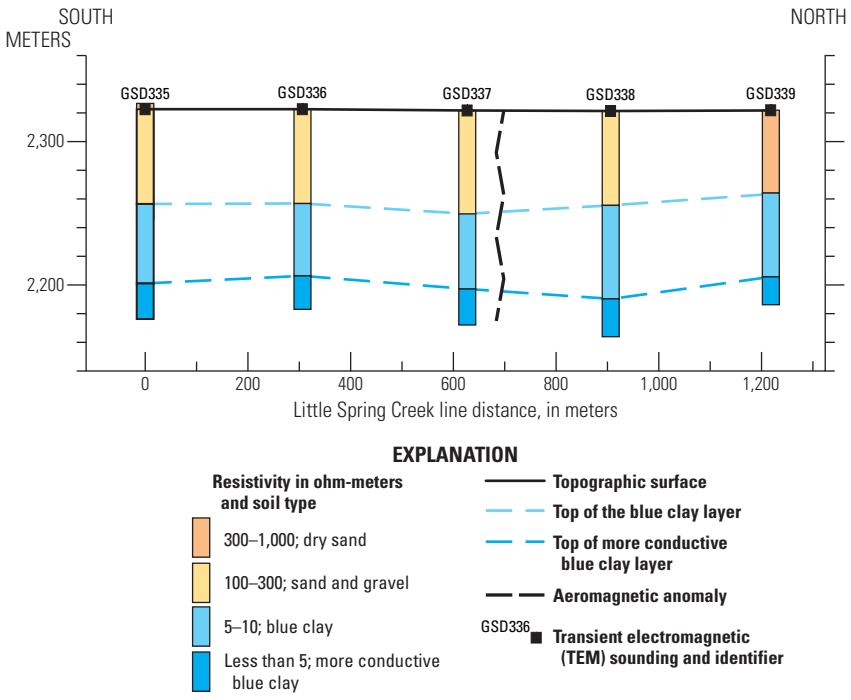

Figure 9. Little Spring Creek line transient electromagnetic (TEM) cross section. The dashed blue lines mark the tops of the blue clay and the deeper, more conductive unit. The wavy, dashed black line locates an aeromagnetic anomaly that could be caused by a fault or old river channel (see figure 3) (V.J.S. Grauch, U.S. Geological Survey, written commun., 2015).

Suspected Valley-Margin Blanca Piedmont Faults

Six TEM profiles were made across faults identified by aeromagnetic data (Grauch and others, 2010) and named the Blanca piedmont fault system (Grauch and others, 2013). The locations of the profiles (lines P1 through P6) can be found in figure 10. Cross sections from the interpreted TEM sounding profiles are shown in figures 11 through 16. The presence and location of a moderately conductive (10–30 ohm-m) zone, interpreted to be a mix of sand and clay, is noted in each profile.

Line P1

Line P1 consists of eight soundings on an east-west line (see fig. 11). The western five soundings are modeled with a four-layer model consisting of a very resistive (greater than 1,000 ohm-m) surface layer and, with the exception of GSD201, are underlain by a moderately resistive (30–100 ohm-m) layer. These two units are interpreted to be dry sand and a sand and gravel mixture, respectively. The third layer is the previously mentioned moderately conductive zone. For two soundings at the middle of the line (GSD204 and GSD205), the bottom of the moderately conductive layer is detected; however, at the eastern three soundings of the line, the moderately conductive layer is absent. The termination of this 10- to 30-ohm-m layer corresponds fairly well with the fault detected by aeromagnetic measurements (wavy, dashed red line in fig. 11).

Line P2

Line P2 is similar to line P1 in that the first five soundings detected the moderately conductive zone, while the last four soundings closest to the mountain front did not (fig. 12). The termination of the conductor is a bit to the southeast of the interpreted fault location. The top of the conductor is relatively flat; however, between soundings GSD221 and GSD222, its elevation increases by 20 m. The location of the fault corresponds to this increase in elevation. A second fault is located between soundings GSD224 and GSD225. The only significant difference in soundings on either side of this location is an increase in the thickness of the resistive surface layer to the southeast. Of and by itself, the increased thickness of the resistive surface layer does not suggest the presence of a fault.

Line P3

Again, the moderately conductive zone is detected at all but the two most easterly soundings (fig. 13). The aeromagnetically detected fault near the location of sounding GSD211 does not correspond to any significant change in resistivity structure; however, between soundings GSD213 and GSD214, there is a jump in the elevation of the conductor. The conductor terminates between soundings GSD215 and GSD216, which corresponds to a fault identified from the aeromagnetic data.

Line P4

The moderately conductive zone is relatively flat on the west end of the line through sounding GSD231 (fig. 14). To the east of GSD231, there is a marked decrease in elevation of the top of the conductive zone, and at GSD232, the bottom of the conductor is detected. These features suggest a fault between soundings GSD231 and GSD232. The aeromagnetic data, however, placed faults near sounding GSD229 and between soundings GSD233 and GSD234. At GSD234, the conductive zone is again detected at a much lower elevation than seen in the other soundings, supporting the fault interpretation.

Line P5

The moderately conductive zone is seen in all the TEM interpretations on this line, and the elevation of the conductor is relatively constant. An aeromagnetically detected fault is located near sounding GSD236; however, the TEM interpretation does not suggest the presence of a fault.

Line P6

The four western soundings on this line clearly detect the blue clay as the deepest layer. At sounding GSD249, though the deepest layer's resistivity is low, it is not low enough to be classified as the blue clay. The base of the moderately conductive (10–30 ohm-m) layer also rises at sounding GSD249 and to the east. These two observations suggest that a lateral transition of some sort is present. The interpretation of the aeromagnetic data puts a fault at sounding GSD248. The dashed green line in the cross section connects a 20-ohm-m layer whose elevation starts to decrease east of sounding GSD249. The lateral changes in the blue clay and the 20-ohm-m layer suggest the presence of a fault between soundings GSD248 and GSD249.

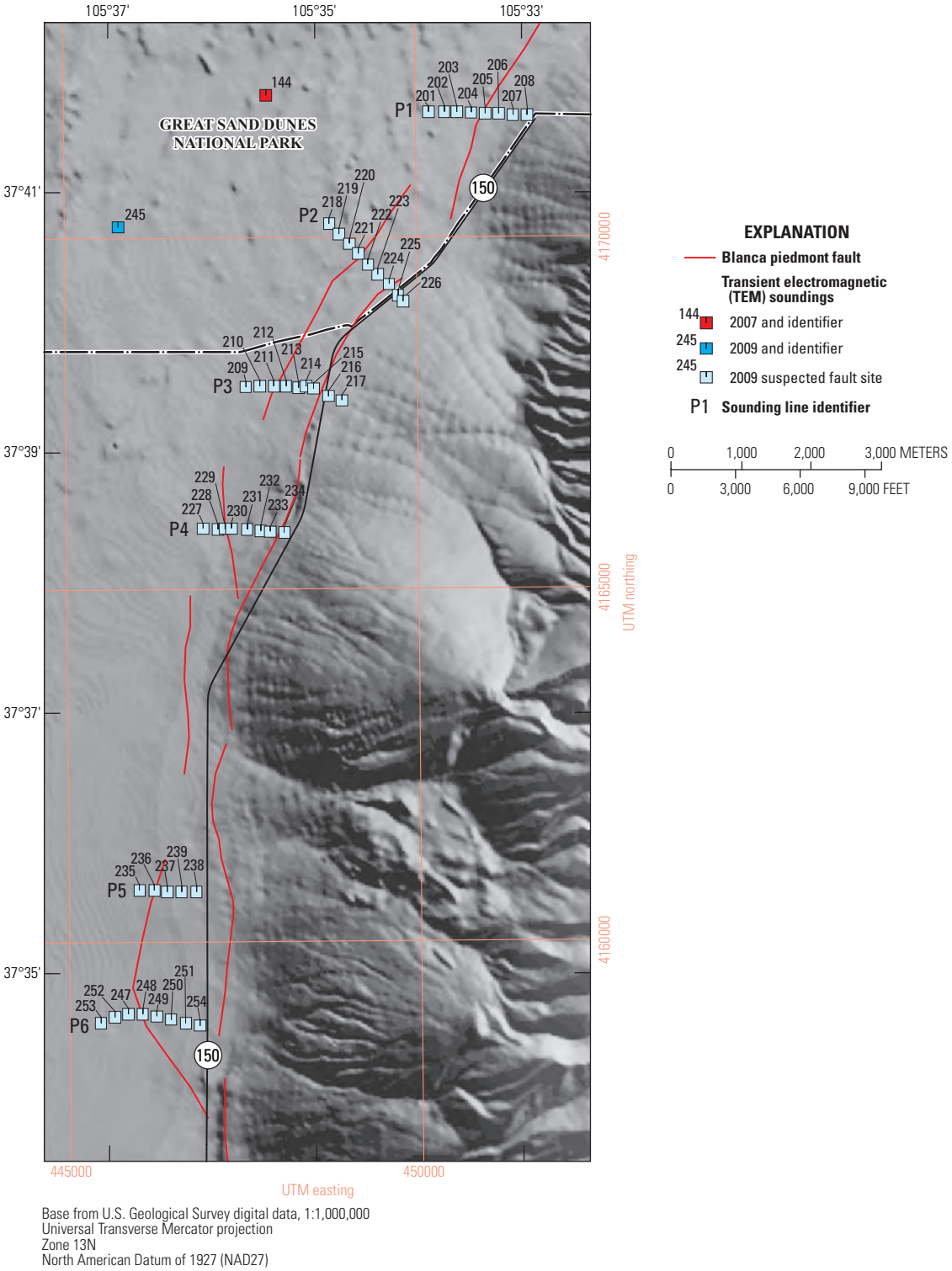

Base from U.S. Geological Survey digital data, 1:1,000,000
Universal Transverse Mercator projection
Zone 13N
North American Datum of 1927 (NAD27)

Figure 10. Location of transient electromagnetic (TEM) profiles (light blue squares) used to investigate the Blanca piedmont fault zone. For clarity, the prefix GSD was removed from sounding identifiers. Red lines mark aeromagnetically mapped faults (Grauch and others, 2010, 2013). The TEM cross sections from these profiles (sounding lines P1 through P6) are shown in figures 11 through 16. See figure 2 for location relative to other study areas. (UTM, Universal Transverse Mercator, in meters)

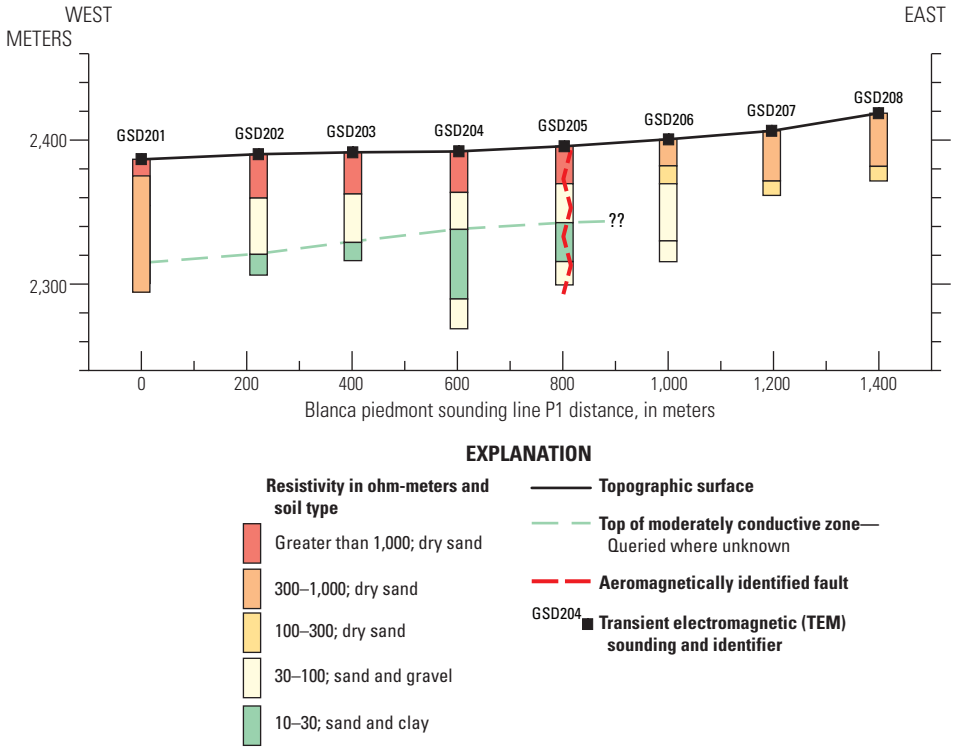

Figure 11. Transient electromagnetic (TEM) cross section for sounding line P1 across a suspected fault. The dashed green line marks the top of a moderately conductive zone. The wavy, dashed red line is an aeromagnetically identified fault (Grauch and others, 2010, 2013).

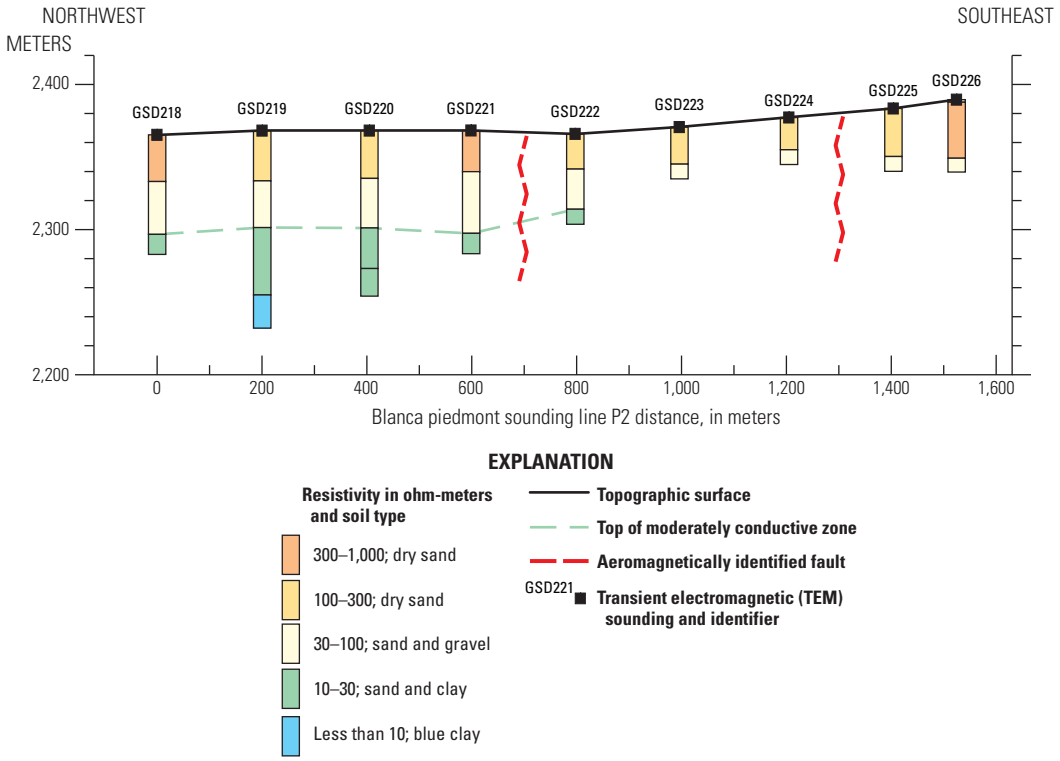

Figure 12. Transient electromagnetic (TEM) cross section for sounding line P2 across suspected faults. The dashed green line marks the top of a moderately conductive zone. The wavy, dashed red lines are aeromagnetically identified faults (Grauch and others, 2010, 2013).

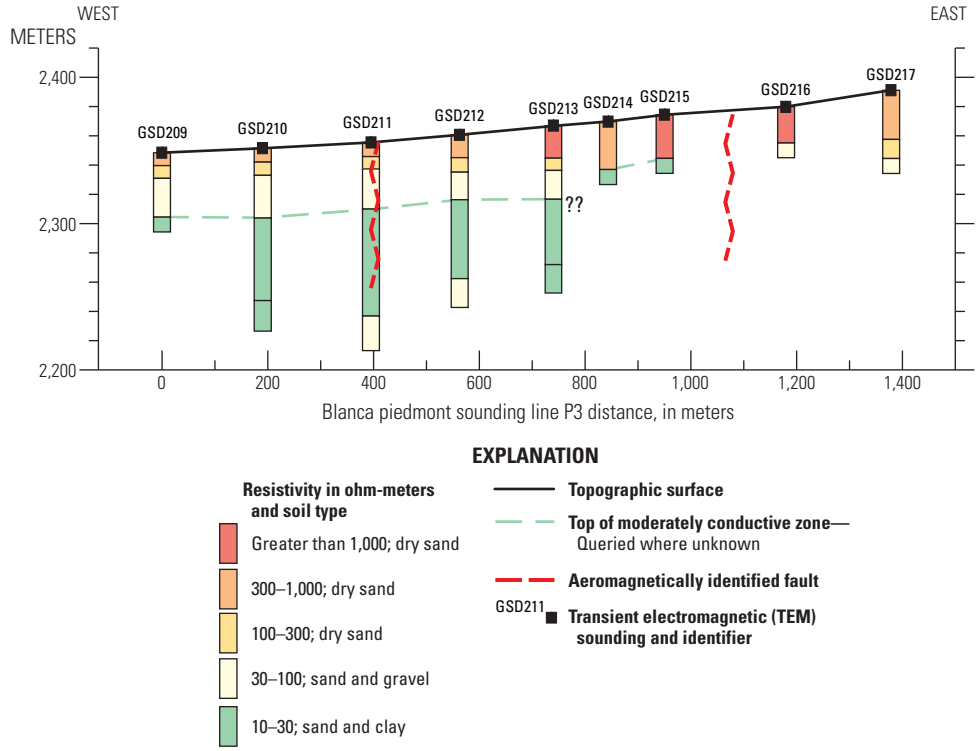

Figure 13. Transient electromagnetic (TEM) cross section for sounding line P3 across suspected faults. The dashed green line marks the top of a moderately conductive zone. The wavy, dashed red lines are aeromagnetically identified faults (Grauch and others, 2010, 2013).

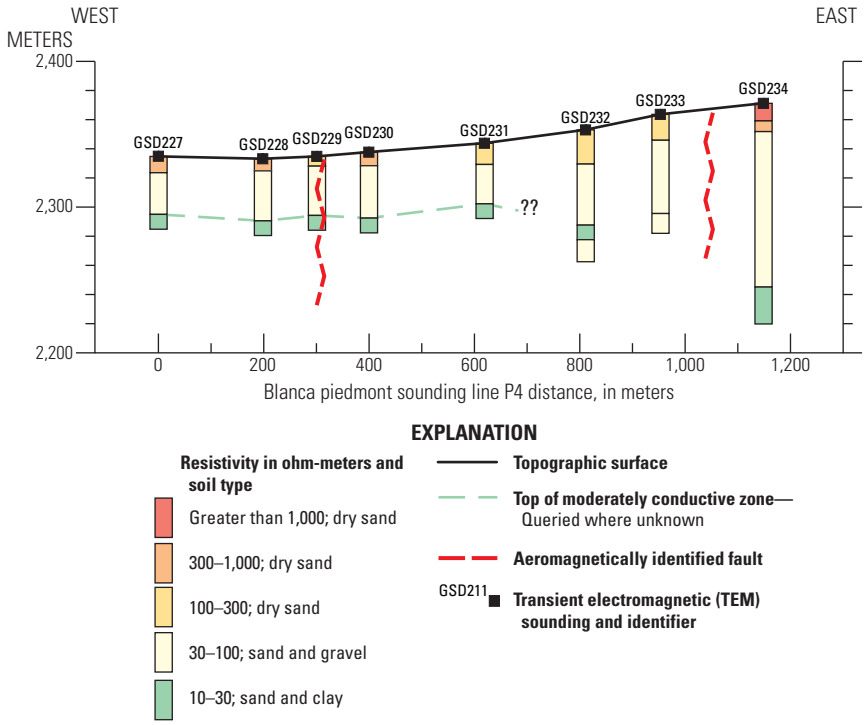

Figure 14. Transient electromagnetic (TEM) cross section for sounding line P4 across suspected faults. The dashed green line marks the top of a moderately conductive zone. The dashed, wavy red lines are aeromagnetically identified faults (Grauch and others, 2010, 2013).

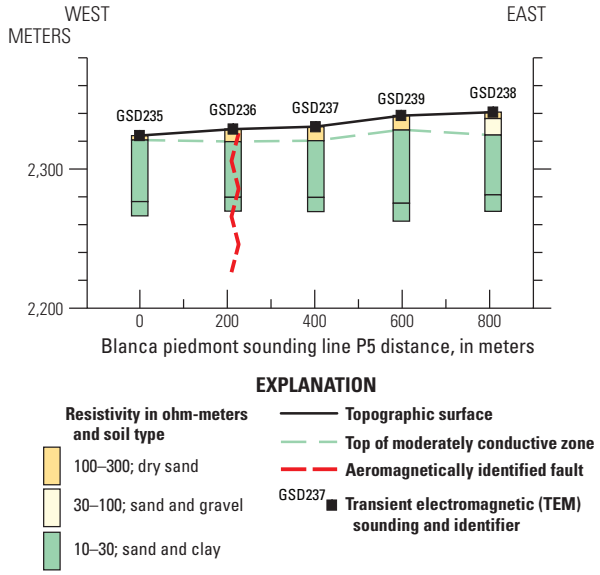

Figure 15. Transient electromagnetic (TEM) cross section for sounding line P5 across a suspected fault. The dashed green line marks the top of a moderately conductive zone. The wavy, dashed red line is an aeromagnetically identified fault (Grauch and others, 2010, 2013).

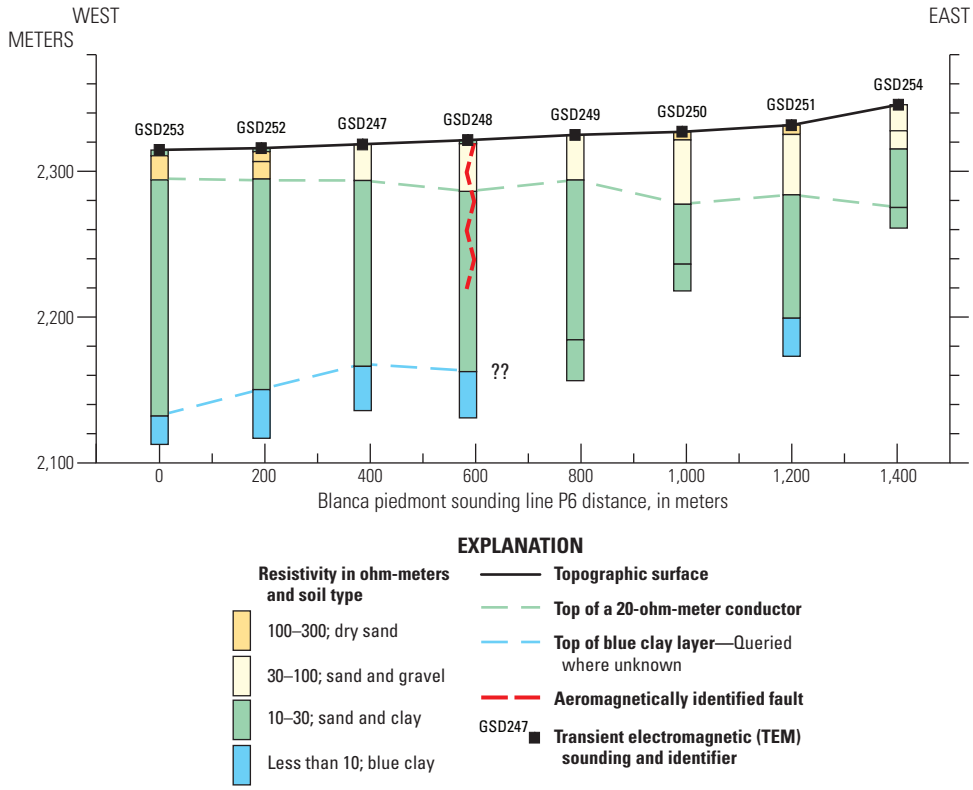

Figure 16. Transient electromagnetic (TEM) cross section for sounding line P6 across a suspected fault. The dashed blue line is the top of the blue clay layer. The dashed green line marks the top of a 20-ohm-meter conductor. The wavy, dashed red line is an aeromagnetically identified fault (Grauch and others, 2010, 2013).

Hansen Bluff Line

A sequence of six TEM soundings were acquired along an east-west line near Hansen Bluff in the Alamosa National Wildlife Refuge (fig. 17). The results presented here are based on the data sets NWR01X through NWR06X, which used turnoff-time adjusted EM-57 data as described in appendix 1. The suffix "X" has been removed from the sounding names in the paragraphs below and in figures 17 and 18. The west end of the line is on a relatively flat area below the scarp that forms the bluff, while the easternmost sounding is on the elevated surface to the east of the scarp. All soundings on the profile detected a very thin resistive surface layer underlain by a 10- to 20-m-thick conductive (less than 10 ohm-m) layer (see fig. 18); the conductive layer at soundings NWR03 and NWR02, however, is much thinner than at the other soundings. At the western three soundings (NWR06 through NWR04), a moderately conductive zone (20–30 ohm-m) was found below the shallow conductor. The top of the moderately conductive zone is fairly level, though its base, the top of the deepest layer (10–20 ohm-m), increases in elevation in the easterly direction by more than 50 m over a distance of 650 m. At soundings NWR03 and NWR02, the third and fourth layers are moderately conductive (10–30 ohm-m) and moderately resistive (30–100 ohm-m), respectively, a pattern which differs from the three western soundings. At the easternmost sounding (NWR01), the very conductive second layer is thick, more similar to the western three soundings; however, the moderately resistive zone seen in soundings NWR03 and NWR02 is present.

This profile was made to investigate a fault identified with aeromagnetic data to the west of Hansen Bluff (fig. 17), near distance 700 m on the profile (fig. 18). The variation in the moderately conductive zone seen between soundings NWR04 and NWR03 suggests the presence of a fault. Between soundings NWR02 and NWR01, the rise in the conductive layers found below the moderately resistive (30–100 ohm-m) layer also suggests faulting. The thickening of the resistive zone at soundings NWR03 and NWR02 just to the west suggests an increased thickness of sand or alluvial material.

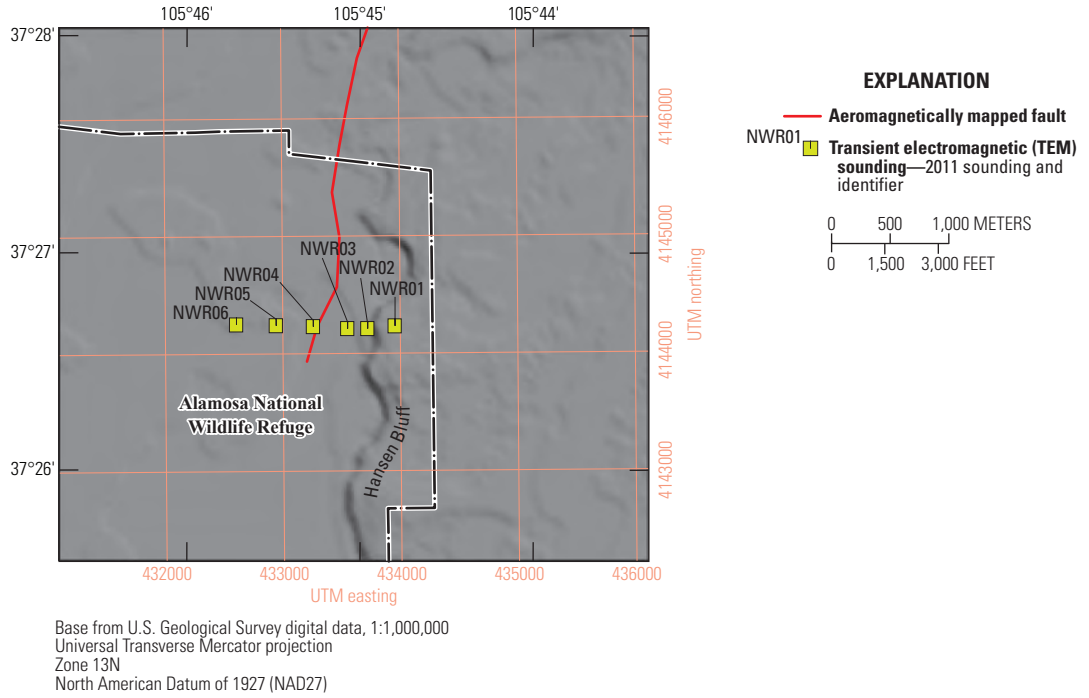

Base from U.S. Geological Survey digital data, 1:1,000,000
Universal Transverse Mercator projection
Zone 13N
North American Datum of 1927 (NAD27)

Figure 17. Location of transient electromagnetic (TEM) soundings near Hansen Bluff, Alamosa National Wildlife Refuge. The red line is a fault interpreted from aeromagnetic data (V.J.S. Grauch, U.S. Geological Survey, written commun., 2015). See figure 2 for location relative to other study areas. (UTM, Universal Transverse Mercator, in meters)

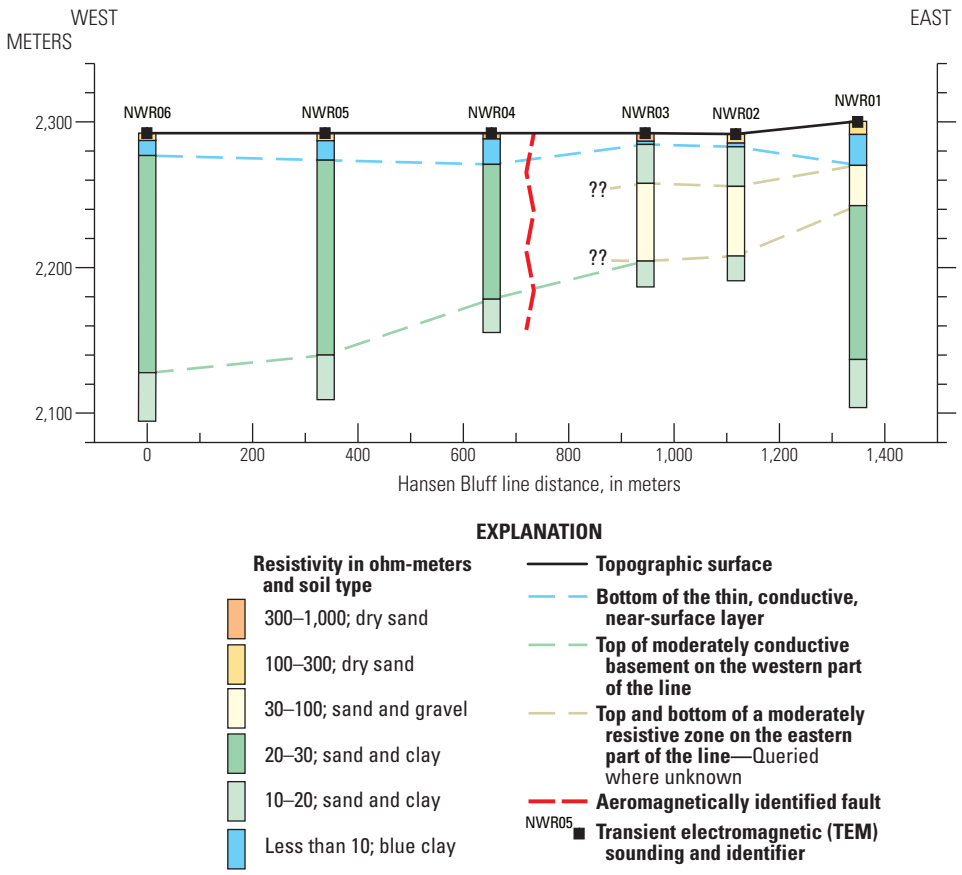

Figure 18. Transient electromagnetic (TEM) cross section along the Hansen Bluff profile. The dashed blue line marks the bottom of the thin, conductive, near-surface layer. The dashed green line marks the top of the moderately conductive (10–20 ohm-meters) basement on the western part of the line. The dashed tan lines mark the top and bottom of a moderately resistive (30–100 ohm-meters) zone on the eastern part of the line. The wavy, dashed red line is an aeromagnetically interpreted fault located near distance 700 meters (V.J.S. Grauch, U.S. Geological Survey, written commun., 2015).

Conclusions

Transient electromagnetic soundings made in the San Luis Valley within and to the west of Great Sand Dunes National Park and Preserve have made it possible to map the depth and elevation of the blue clay that forms the base of the unconfined aquifer. A resistivity criterion of 10 ohm-meters or less, based on analysis of well logs, was used to identify the clay zone. The relief of the clay surface suggests that the clay was deposited on an existing topographic relief and (or) that there was deformation of the clay during or after deposition at the bottom of ancient Lake Alamosa. As this region has been tectonically active, the deformation of sediments in the Alamosa Formation is to be expected. Lake Alamosa covered much of the San Luis Valley until middle Pleistocene time (Machette and others, 2007). Several profiles along the eastern edge of the valley inside and south of the Great Sand Dunes National Park and Preserve near the mountain front were made across the Blanca piedmont fault zone, identified using aeromagnetic data (Grauch and others, 2010). In most cases, lateral discontinuities of conductive zones were detected that could be interpreted as faulting. These changes in resistivity structure were usually near the aeromagnetically determined faults, though sometimes they were separated by 100–200 meters.

An additional profile made across Hansen Bluff in the Alamosa National Wildlife Refuge found lateral changes in the resistivity structure across the bluff. There is a marked increase in elevation of a conductive zone as the bluff is approached from the west from the level of the Rio Grande. Corresponding to this elevation transition is the introduction of a moderately resistive layer in the sounding models. Both of these features support the aeromagnetic interpretation and the possibility of faulting associated with the bluff; however, they do not conclusively prove its existence.

Acknowledgments

Andrew Valdez and Fred Brunch (National Park Service) were invaluable in gaining access to Great Sand Dunes National Park and Preserve and the Mendano-Zapata Ranch, familiarizing U.S. Geological Survey (USGS) personnel with the area, and assisting with field operations including the retrieval of stuck vehicles. Ron Garcia (U.S. Fish and Wildlife Service) facilitated access to U.S. Fish and Wildlife Service lands including the Baca National Wildlife Refuge and the Alamosa National Wildlife Refuge. Data collection would not have been possible without the effort of Chad Ailes (USGS), Jay Sampson (USGS), Calvin Johnson (UNAVCO), and Daniel Labson (USGS). Discussions with Tien Grauch (USGS) provided important information about aeromagnetic and drill hole data that helped guide the direction of this work. Review comments by Burke Minsley (USGS) and Ben Drenth (USGS) helped improve the report.

References Cited

Colorado District Court Water Division No. 3, 2004, Case 2004CW35—In the matter of the application for water rights of the United States of America in Alamosa and Saguache Counties. Findings of fact, conclusions of law, judgement and decree: District Court, Water Division No. 3, Colorado, August 4, 2008, 22 p.

Fitterman, D.V., 1989, Detectability levels for central induction transient soundings: Geophysics, v. 54, no. 1, p. 127–129.

Fitterman, D.V., 2016, Transient electromagnetic sounding data collected in the San Luis Valley, Colorado, near the Great Sand Dunes National Park and Preserve and the Alamosa National Wildlife Refuge (field seasons 2007, 2009, and 2011): U.S. Geological Survey data release, accessed December 2016 at https://doi.org/10.5066/F7D21VQ5.

Fitterman, D.V., and de Souza Filho, O.A., 2009, Transient electromagnetic soundings near Great Sand Dunes National Park and Preserve, San Luis Valley, Colorado (2006 field season): U.S. Geological Survey Open-File Report 2009–1051, 63 p. [Also available at http://pubs.usgs.gov/of/2009/1051/.]

Fitterman, D.V., Deszcz-Pan, Maria, and Stoddard, C.E., 1999, Results of time-domain electromagnetic soundings in Everglades National Park, Florida [CD-ROM]: U.S. Geological Survey Open-File Report 99–426, 152 p.

Fitterman, D.V., and Grauch, V.J.S., 2010, Transient electromagnetic mapping of clay units in the San Luis Valley, Colorado, in 23rd Symposium on the Application of Geophysics to Engineering and Environmental Problems (SAGEEP 2010), Keystone Colo., April 11–15, 2010, Proceedings: Environmental and Engineering Geophysical Society, p. 154–164.

Fitterman, D.V., and Labson, V.F., 2005, Electromagnetic induction methods for environmental problems, *in* Butler, D.K., ed., Near surface geophysics—Part 1. Concepts and fundamentals: Tulsa, Okla., Society of Exploration Geophysicists, p. 295–349.

Fitterman, D.V., and Stewart, M.T., 1986, Transient electromagnetic sounding for groundwater: Geophysics, v. 51, p. 995–1005.

Goldman, M., Gilad, D., Ronen, A., and Melloul, A., 1991, Mapping seawater intrusion into the coastal aquifer of Israel by the time domain electromagnetic method: Geoexploration, v. 28, p. 153–174.

Grauch, V.J.S., Bedrosian, P.A., and Drenth, B.J., 2013, Advancements in understanding the aeromagnetic expressions of basin-margin faults—An example from the San Luis Basin, Colorado: The Leading Edge, v. 32, no. 8, p. 882–891.

Grauch, V.J.S., Fitterman, D.V., and Drenth, B.J., 2010, Finding faults using high-resolution aeromagnetic data in Great Sand Dunes National Park and vicinity, San Luis Valley, Colorado, in 23rd Symposium on the Application of Geophysics to Engineering and Environmental Problems (SAGEEP 2010), Keystone Colo., April 11–15, 2010, Proceedings: Environmental and Engineering Geophysical Society, p. 428–437.

Grauch, V.J.S., Skipp, G.L., Thomas, J.V., Davis, J.K., and Benson, M.E., 2015, Sample descriptions and geophysical logs for cored well BP-3-USGS, Great Sand Dunes National Park, Alamosa County, Colorado: U.S. Geological Survey Data Series, 918, 53 p. [Also available at https://doi.org/10.3133/ds918.]

Hohmann, G.W., and Raiche, A.P., 1988, Inversion of controlled-source electromagnetic data, *in* Nabighian, M.N., ed., Electromagnetic methods in applied geophysics—Volume 1. Theory: Tulsa, Okla., Society of Exploration Geophysicists, p. 468–504.

HRS Water Consultants Inc., 1999, Hydrogeologic investigations Sand Creek and Indian Springs area, Great Sand Dunes National Monument, Colorado: Report to National Park Service, May 1999, 92021-04, 40 p.

HRS Water Consultants Inc., 2009, Documentation of boundary piezometer installation, Great Sand Dunes National Park and Preserve, Colorado: Report to U.S. Department of Justice and National Park Service, December 2009, HRS Project 04-06.10.

Huntley, David, 1979, Cenozoic faulting and sedimentation in northern San Luis Valley, Colorado: Geological Society of America Bulletin, Part II, v. 90, no. 1, p. 135–153.

Kaufman, A.A., and Keller, G.V., 1983, Frequency and transient sounding: Amsterdam, Elsevier, 685 p.

Machette, M.N., 2004, New evidence for ancient Lake Alamosa in the San Luis Basin of Colorado: Geological Society of America Abstracts with Program, v. 36, no. 5, p. 530.

Machette, M.N., Marchetti, D.W., and Thompson, R.A., 2007, Ancient Lake Alamosa and the Pliocene to middle Pleistocene evolution of the Rio Grande, chap. G *of* Machette, M.N., Coates, M.-M., and Johnson, M.L., eds., 2007 Rocky Mountain Section Friends of the Pleistocene Field Trip—Quaternary geology of the San Luis Basin of Colorado and New Mexico, September 7–9, 2007: U.S. Geological Survey Open-File Report 2007–1193, p. 157–167.

Machette, M.N., Thompson, R.A., Marchetti, D.W., and Smith, R.S.U., 2013, Evolution of ancient Lake Alamosa and integration of the Rio Grande during the Pliocene and Pleistocene, *in* Hudson, M.R., and Grauch, V.J.S., eds., New perspectives on Rio Grande rift basins—From tectonics to groundwater: Geological Society of America Special Paper 494, p. 1–20.

McNeill, J.D., 1990, Use of electromagnetic methods for groundwater studies, *in* Ward, S.H., ed., Geotechnical and environmental geophysics: Tulsa, Okla., Society of Exploration Geophysicists, p. 191–218.

Oldenburg, D.W., and Li, Yaoguo, 2005, Inversion for applied geophysics—A tutorial, *in* Butler, D.K., ed., Near surface geophysics—Part 1. Concepts and fundamentals: Tulsa, Okla., Society of Exploration Geophysicists, p. 89–150.

Siebenthal, C.E., 1910, Geology and water resources of the San Luis Valley, Colorado: U.S. Geological Survey Water-Supply Paper 240, 128 p.

Valdez, Andrew, 2007, Stop A8—Closed basin overflow and origin of Hansen Bluff, *in* Machette, M.N., Coates, M.-M., and Johnson, M.L., eds., 2007 Rocky Mountain Section Friends of the Pleistocene Field Trip—Quaternary geology of the San Luis Basin of Colorado and New Mexico, September 7–9, 2007: U.S. Geological Survey Open-File Report 2007–1193, p. 38–39.

Appendix 1. Description of Transient Electromagnetic (TEM) Data Processing

Processing of the transient electromagnetic (TEM) data included the following steps: (1) downloading, (2) averaging, (3) inversion, (4) extracting results, (5) plotting, and (6) report generation. Figure 1–1 summarizes the data flow and processing programs used. The data in the Geonics Limited PROTEM-D receiver are downloaded to a PC using program PROTEM, which is supplied by Geonics Limited. Typically, data from one sounding location are downloaded into a single raw data file (filename extension .TEM). The format of this file is referred to as the Geonics TEM File (GTF) format. It is described in detail in appendix 2 below. After downloading, selected data records from the raw data file are averaged using the program DTEMAVG. (The program NTEMAVG was used for the 2009 data collected with an analog PROTEM receiver.) Data are usually selected to include measurements made with the same receiver gain and integration time, though this is not mandatory. The averaged data files (filename extension .TAV) are saved in GTF format. In addition to the averaged data file, a file containing a summary of the averaging process is saved (filename extension .PRV).

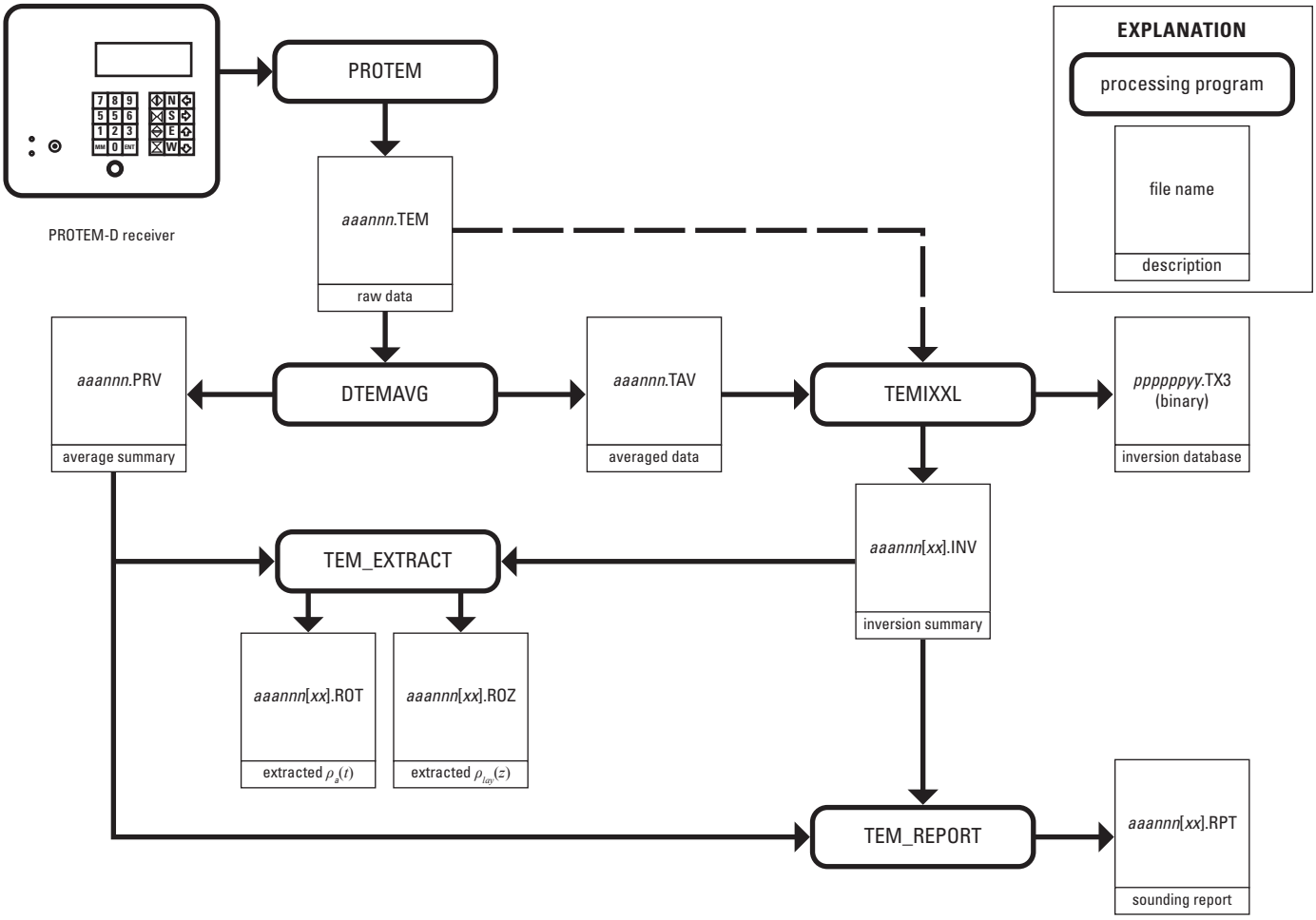

Figure 1–1. Data processing programs, files, and flow. The processing steps and associated programs are as follows: (1) downloading (PROTEM), (2) averaging (DTEMAVG), (3) inversion (TEMIXXL), (4) result extraction (TEM_EXTRACT), and (5) report generation (TEM_REPORT). Detailed descriptions are given in the text. A description of the file formats is given in appendix 2. Solid lines show processing flow; the dashed line is an alternative path. For data from the analog PROTEM receiver, the program NTEMAVG was used to average data instead of DTEMAVG. The program PROTEM is available from Geonics Limited. The program TEMIXXL is available from Interpex Limited. The programs DTEMAVG, NTEMAVG, TEM_EXTRACT, and TEM_REPORT are unpublished software developed at the U.S. Geological Survey. ($\rho_a(t)$, apparent resistivity as a function of time; $\rho_{lay}(z)$, interpreted resistivity as a function of depth)

Both the raw and averaged data files can be read into TEMIXXL, a program commercially available from Interpex Limited, which was used for data interpretation. The TEMIXXL program stores a copy of the data, the model, and the calculated response of the model in a proprietary binary database file (filename extension .TX3). The database can hold a large number of soundings, so one database is usually enough for an entire survey. Sometimes it is helpful to retain several alternative models for a given dataset. These are stored as separate soundings in the TEMIXXL database. Typically, these alternative models have the original sounding name with up to 3 characters added at the end. For example, a sounding called ABC101 might have variants ABC101L4 and ABC101L5 to indicate models with four and five layers, respectively. Soundings that have a fixed-layer resistivity are given names with an "F" after the sounding name, such as ABC101F or ABC104F5. The former name indicates that a layer resistivity is fixed, while the latter is an alternative model with a fixed resistivity and five layers. The only restriction on the extra characters in the sounding name is that the total number of characters in the name cannot exceed 8. The results of the inversion are reported in an inversion output file (filename extension .INV).

The program TEM_EXTRACT is used to extract apparent-resistivity-time (filename extension .ROT) and interpreted-resistivity-depth (filename extension .ROZ) files for plotting. After the interpretation process is completed, a report file (filename extension .RPT) is generated using program TEM_REPORT. This file contains all of the information about sounding parameters, data values, model parameters, and model response. There is adequate information in this file to enter the data into another inversion program to verify the results.

Hansen Bluff Data

The 2011 field season Hansen Bluff data were collected with both the EM-47 and EM-57 configurations. Because the time ranges of these instruments overlap (30-hertz [Hz] base-frequency data), the measurements can be compared. Two issues were discovered in the Hansen Bluff data. The first involved the EM-47 data—the standard deviation of the 30-Hz base-frequency data was about 15 percent at all time gates for soundings NWR03, NWR05, and NWR06. This is unusual in two regards: (1) the standard deviation is expected to be much smaller for this base frequency and (2) the standard deviation usually increases with time and does not stay relatively constant. Examination of the data revealed that the voltage of any particular channel tended to increase between measurements (each measurement is the time averages of several hundred transients) and that the ratio of voltage between consecutive measurements was approximately the same for all channels, but not unity as would be expected, suggesting that the transmitter current was changing in a systematic way.

To test this hypothesis, the ratio of channel voltages between the first and subsequent measurement cycles was computed and averaged. Only data from the first 10, 11, and 8 channels were used in the averages for soundings NWR03, NWR05, and NWR06, respectively, because in later channels the data became noisier. With these initial channels selected, the standard deviation of the channel-averaged voltage ratio was in the range of 0.3–0.7 percent. Plots of the channel-averaged voltage ratio as a function of measurement cycle number are shown in figure 1–2. These curves represent changes in the transmitter current while the set of measurements were being made. Normally, the current is kept constant, but that does not appear to be the case here. It is suspected that the transmitter operator adjusted the current upward on these three soundings for some unknown reason. Dividing the raw data voltages by the voltage ratio resulted in data standard deviations that were more in line with other datasets from this survey.

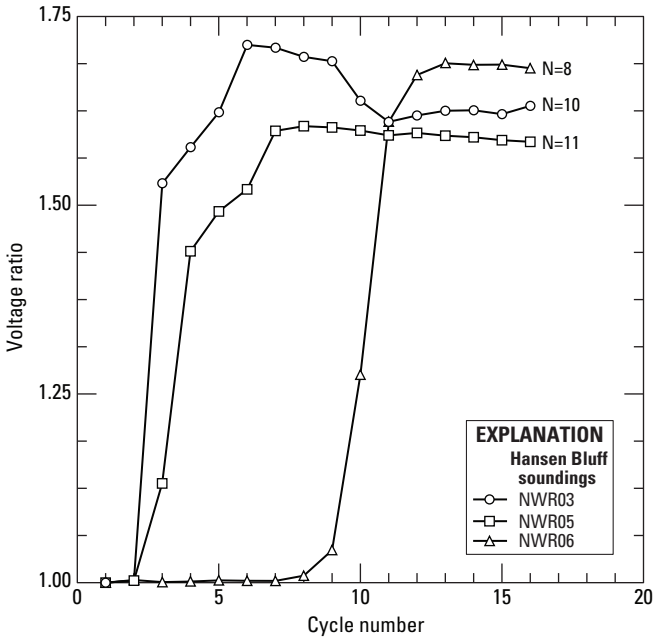

Figure 1–2. Plots of channel-averaged voltage ratio as a function of measurement cycle number for 30-hertz EM-47 data from soundings NWR03, NWR05, and NWR06. The voltage ratio is the voltage of a particular cycle divided by the voltage of the first cycle averaged over the first N channels of the transient. The value of N used for each sounding dataset is indicated in the figure. Voltage ratios greater than 1 indicate an apparent increase of transmitter current.

The second issue involved comparison of the EM-47 and EM-57 data. Plots of the Hansen Bluff apparent resistivity data showed that the first four to ten channels of the 30-Hz EM-57 data ("HI" frequency code) are higher than the corresponding EM-47 data ("hi" frequency code) in the same time range. Attempts to invert the data resulted in models that poorly fitted the observations in this time range, with the model apparent resistivity lying between the EM-57 and EM-47 data. (For plots of soundings NWR01C, NWR02C, NWR03C, NWR04C, NWR05C, and NWR06C see Fitterman [2016], document "TEM_plots_2011.pdf," figs. 9-40b, 9-41b, 9-42b, 9-43b, 9-44b, and 9-45b.) One possible cause could be that the time it takes for the transmitter to turn off is different from the value measured by the EM-57 transmitter. The measured turnoff time is entered into the receiver to delay the start of measurement by the amount of the turnoff time. For the current and loop configuration used for this survey, the measured turnoff time was 36–38 microseconds (μs). Inversion of the combined EM-47 and EM-57 data could not achieve a mutually agreeable model for the two transmitters when this measured turnoff time was used for the EM-57 data. To correct this situation, inversions were made for the Hansen Bluff data using different EM-57 turnoff times to determine the value that gave the minimum misfit error between the data and the inversion model. The manufacturer's specified turnoff time was used for the EM-47 data (2.5 μs). This procedure resulted in very good agreement between the measured and calculated apparent resistivities at all times including the early part of the EM-57 transient. (See Fitterman [2016], document "TEM_plots_2011.pdf," figs. 9-40a, 9-41a, 9-42a, 9-43a, 9-44a, and 9-45a.) The measured and best-fit EM-57 turnoff times are summarized in table 1–1 along with the corresponding misfit error.

Table 1–1. Measured and adjusted EM-57 turnoff time for Hansen Bluff soundings with corresponding misfit error.

[T/O, turnoff time; μs, microsecond; %, percent]

Sounding	Measured T/O (μs)	Measured T/O misfit error (%)	Best-fit T/O (μs)	Best-fit T/O misfit error (%)
NWR01	38	7.41	72.5	1.63
NWR02	36	7.75	70	2.72
NWR03	36	3.93	50	2.61
NWR04	36	4.59	45	2.72
NWR05	35	9.33	75	3.18
NWR06	37	9.96	85	4.26

Appendix 2. Description of Transient Electromagnetic (TEM) Data Files

The file naming conventions and formats of files generated during downloading, processing, inversion, and extraction are described below. All subdirectories referred to in this appendix are located in the data release by Fitterman (2016) that accompanies this data series, in the directory "TEMSLV*yyyy*," where "*yyyy*" is the year the field work was conducted.

File Naming Conventions

The files of downloaded raw data in Geonics TEM File (GTF) format are typically given a name of the form "*aaannn*.TEM," where "*aaa*" is a three-character identifier associated with the survey or the area and "*nnn*" is a three-digit number. The sounding "name" would be considered "*aaannn*." Geonics Limited and some software vendors give these files an extension of .RED, which is not used here.

Files of averaged data are also in the GTF format and have names in the form "*aaannn*.TAV." A printed summary of the averaging process is written to a file with a name in the form "*aaannn*.PRV."

The TEMIXXL database files are used to store transient electromagnetic sounding data. The databases are binary files in a proprietary format with the filename extension .TX3. Each dataset in a TEMIXXL database includes observed data, measurement parameters, calculated model response, and inversion model parameters. A dataset is identified by a name of up to 8 characters. The dataset identifiers are the same as the sounding names, unless it is an alternative model, in which case additional letters are added after the sounding name. The additional letters usually indicate the number of layers in the model (for example, L3 for a three-layer model, or F4 for a four-layer model with a fixed layer resistivity). For the Hansen Bluff data, a suffix of "C" (for combined) indicates that there are EM-47 and EM-57 data in the dataset, and a suffix of "X" indicates that the EM-57 turnoff time has been adjusted in the processing for a better inversion fit. A summary of the inversion is written to a file named in the form "*aaannn*[*xx*].INV," where "[*xx*]" represents optional characters added to the sounding name in TEMIXXL to identify alternative models.

Extracted apparent-resistivity-time and interpreted-resistivity-depth files suitable for plotting are named in the form "*aaannn*[*xx*].ROT" and "*aaannn*[*xx*].ROZ," respectively.

Report files summarizing an individual sounding location, equipment used, data, and inversion model are named in the form "*aaannn*[*xx*].RPT." The individual report files for a field season have been concatenated into a single file and are provided as a text and a portable document format (PDF) file.

File Formats and Contents

(a) Geonics TEM File (GTF) Format

The raw data collected in the field are written in Geonics TEM file (GTF) format. The GTF files consist of records 256 characters long containing a 50-character header field followed by 25 data fields of 8 characters each. A 4-character sequential record number follows the last data field. The last 2 characters of the record are a carriage return and a line feed. Two types of records are created during PROTEM-D receiver downloading. The record type is indicated by characters 19–21 of the header field: "HDR" for a header record and "OPR" for a data record. A header record is created every time a change is made in certain measurement parameters in the PROTEM-D receiver. For example, changes in the sounding name, transmitter current, transmitter loop size, turnoff time, or receiver moment will produce a new header record.

The raw data files from this survey can be found in the data release subdirectory "RAW_DATA" (Fitterman, 2016).

Digital PROTEM-D File Format (extension .TEM)

Figure 2–1 shows the structure of the digital PROTEM-D receiver header fields for header (HDR) and data (OPR) records; descriptions for these two types of header fields are given in tables 2–1 and 2–2, respectively.

The data fields of header and data records contain 25 eight-character data fields. Geonics Limited's documentation refers to these data fields as gates. The contents of the gates are given in tables 2–3 and 2–4 for header and data records, respectively.

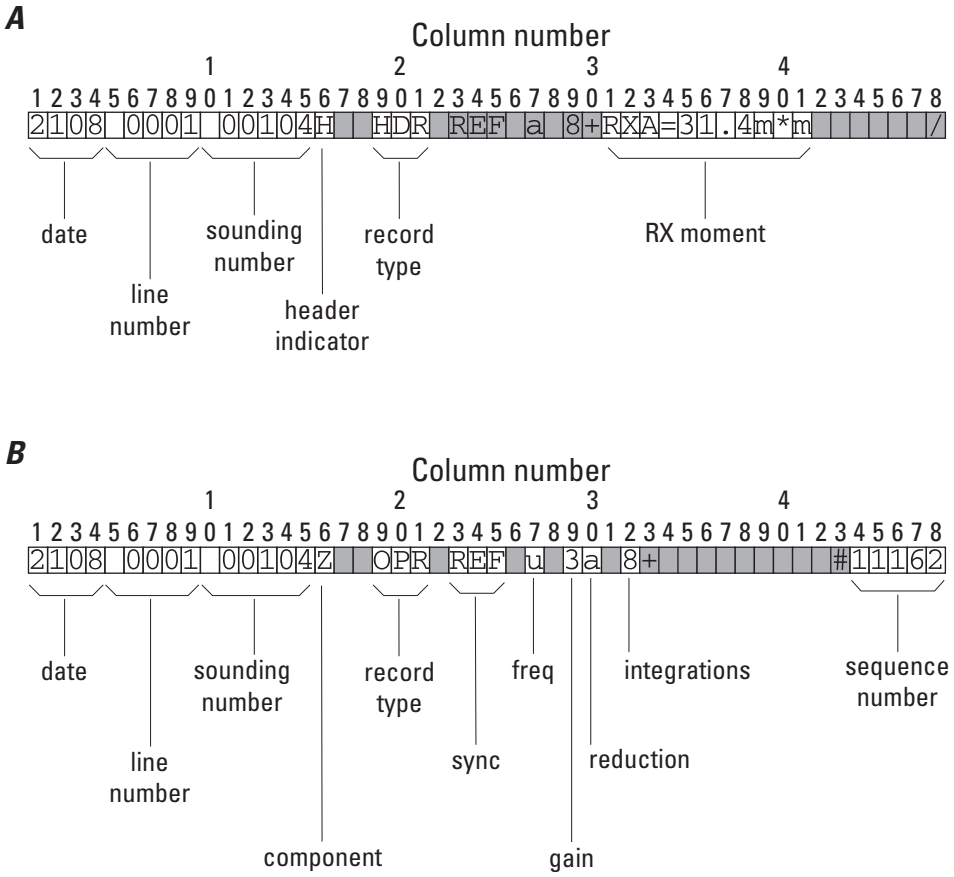

Figure 2–1. Diagram showing contents of the digital PROTEM-D receiver header fields. The contents of shaded cells are ignored in further processing. *A*, Header record (HDR), header fields. (RX, receiver) *B*, Data record (OPR), header fields.

Table 2–1. Description of the digital PROTEM-D receiver header record (HDR) header fields (see figure 2–1*A*).

Field	Columns	Description
date	1–4	date of measurement; usually in day-month format (ddmm), but format depends on particular receiver used
line number	5–9	set by operator; usually set to the sounding number
sounding number	10–15	set by operator to identify the sounding
header indicator	16	"H" to indicate header record
record type	19–21	"HDR" to indicate header record
RX moment	31–41	receiver (RX) coil moment (turn•square meter)

Table 2–2. Description of the digital PROTEM-D receiver data record (OPR) header fields (see figure 2–1*B*).

Field	Columns	Description
date	1–4	date of measurement; usually in day-month format (ddmm), but format depends on particular receiver used
line number	5–9	set by operator; often the same as the sounding number
sounding number	10–15	sequence number of sounding; requires operator to manually update or values will not be significant
component	16	indicates measured component: X, Y, or Z
record type	19–21	"OPR" to indicate data record
sync	23–25	synchronization method; "REF" indicates reference cable, "XTL" indicates crystal oscillators
freq	27	transmitter (TX) repetition frequency; determines measurement times. For EM-47 TX: u, ultra high; v, very high; h, high. For EM-57 TX: H, high; M, medium; L, low
gain (G)	29	adjustable PROTEM gain factor; actual gain is 2^G
reduction	30	value of "a" indicates that receiver 4× and 10× gain factors have been removed
integrations	32	PROTEM coded integration time setting
sequence number	44–48	sequence number of data record (nnnnn)

Table 2–3. Description of the digital PROTEM-D receiver header record (HDR) data fields (gates).

[TX, transmitter; RX, receiver]

Field (gate)	Contents
0	date of measurement in month-day format (mmdd)
2	time of measurement in hour-minute format (hhmm)
4	TX current (ampere)
5	TX turnoff time (microsecond)
6–7	TX loop side length LX (meter) and LY (meter)
8–9	RX coil position XR (meter) and YR (meter) relative to center of TX loop
10	RX coil moment (turn•square meter)
11	TX number (47 or 57)
22	logger record number for this header record

Analog PROTEM File Format (extension .TEM)

Figure 2–2 shows the structure of the analog PROTEM receiver header fields for header (HDR) and data (OPR) records; descriptions for these two types of header fields are given in tables 2–5 and 2–6, respectively.

The data fields of header and data records contain 25 eight-character data fields. Geonics Limited's documentation refers to these data fields as gates. The contents of the gates are given in tables 2–7 and 2–8 for header and data records, respectively.

Averaged Data File Format (extension .TAV)

The files that contain the averaged data have the filename extension .TAV and use the GTF format. The header of the first record indicates the type of instrument the data came from and whether the data have been averaged. If the PROTEM-D digital receiver was used, the header reads "Data from Geonics TEM58 RX. -- AVERAGED"; if the PROTEM analog receiver was used, the header reads "Geonics EMx7 TEM data from PROTEM -- AVERAGED." The data fields of this record are all set to zero. The second record is an HDR record with header fields and data fields as described in tables 2–1 and 2–3 for PROTEM-D data and tables 2–5 and 2–7 for PROTEM data. Next comes an OPR record for each frequency average computed by the program DTEMAVG (or NTEMAVG for data recorded with an analog receiver). If different groups of data records were averaged, there will be multiple output records—one for each group. Following the last OPR record comes a record whose header field starts with "XXXXX." The numbers in the data fields are meaningless.

The averaged data files (.TAV files) from this survey can be found in the data release subdirectory "AVG_DATA" (Fitterman, 2016).

Table 2–4. Description of the digital PROTEM-D receiver data record (OPR) data fields (gates).

[TEM, transient electromagnetic; TX, transmitter; RX, receiver]

Field (gate)	Contents
0	primary field value
1–20	channels 1–20 TEM data (millivolt)
21	TX turnoff time (millisecond)
22	first RX gate time (millisecond)
23	TX current (ampere)
24	TX moment (turn•square meter), may include a trailing "/"
25	time of measurement in hour-minute format (hhmm)

(b) Averaging Process Summary Files (extension .PRV)

The text files that summarize the data averaging process have the filename extension .PRV. The first page of the file consists of a listing of all of the header record (HDR) and data record (OPR) header fields. The first line is a descriptive header indicating with which receiver type the data were collected. If the PROTEM-D digital receiver was used, the header reads "Data from Geonics TEM58 RX"; if the PROTEM analog receiver was used, the header reads "Geonics EMx7 TEM data from PROTEM logger." The second line usually contains HDR header fields. Subsequent lines are OPR header fields associated with the recorded data. Additional HDR header fields will be present if the operator made a change in the header information on the receiver. The output concludes with a record whose header field starts with "XXXXXX" to indicate the end of the data processing.

Following the summary page, a separate page is devoted to data records that were averaged together. There is usually one page for each transmitter repetition frequency used for the sounding. The first line of these pages indicates the program version used to average the data, the averaged-output file name, the record number of the averaged-output file to which this page corresponds, and the GTF-format input file name.

Each data page of the .PRV file contains a summary of all of the data recorded by the receiver for a single frequency. For each measurement, there is a data record number (DRN), frequency (FREQ), transmitter current (CUR), receiver gain (GAIN), integrations value (NSTK), transmitter turnoff time (T/O), and a time shift (SHIFT). The time shift is applied during data averaging to adjust for incorrect turnoff time settings during data recording. If no adjustment was made, this value will be zero. This part of the output is followed by a list of the International System (SI) units of the various reported quantities, the transient electromagnetic (TEM) instrument (receiver) used (EM-58 for the PROTEM-D and EM-x7 for the analog PROTEM), the receiver coil moment (RXA), the transmitter loop dimensions (LX and LY), and the location of the receiver coil with respect to the center of the transmitter loop (XR and YR).

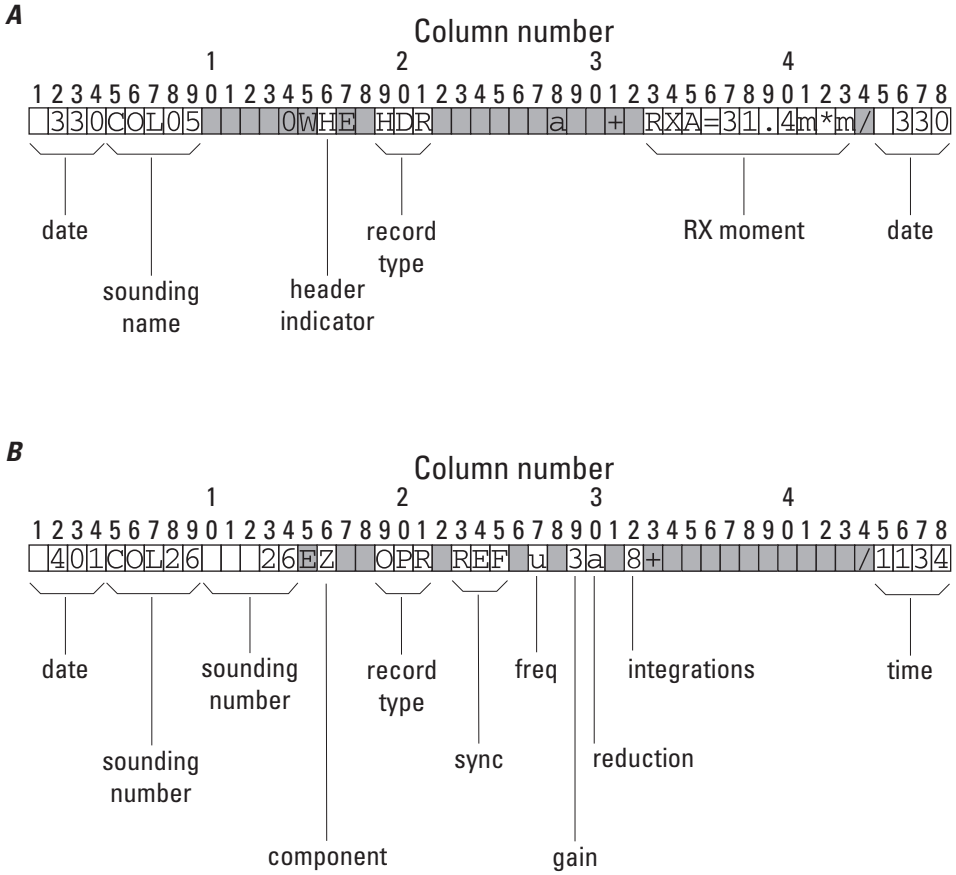

Figure 2–2. Diagram showing contents of the analog PROTEM receiver header fields. The contents of shaded cells are ignored in further processing. *A*, Header record (HDR), header fields. (RX, receiver) *B*, Data record (OPR), header fields.

Table 2–5. Description of the analog PROTEM receiver header record (HDR) header fields (see figure 2–2*A*).

Field	Columns	Description
date	1–4	date of measurement; usually in month-day format (mmdd), but format depends on particular receiver used
sounding name	5–9	sounding name
header indicator	16	"H" to indicate header
record type	19–21	"HDR" to indicate header record
RX moment	33–43	receiver (RX) coil moment (turn•square meter)
date	45–48	date of measurement in month-day format (mmdd)

Table 2–6. Description of the analog PROTEM receiver data record (OPR) header fields (see figure 2–2*B*).

Field	Columns	Description
date	1–4	date of measurement; usually in month-day format (mmdd)
sounding name	5–9	sounding name
sequence number	10–14	sequence number of sounding; requires operator to manually update or values will not be significant
component	16	indicates measured component: X, Y, or Z
record type	19–21	"OPR" to indicate data record
sync	23–25	synchronization method; "REF" indicates reference cable, "XTL" indicates crystal oscillators
freq	27	transmitter (TX) repetition frequency; determines measurement times. For EM-47 TX: u, ultra high; v, very high; h, high. For EM-57 TX: H, high; M, medium; L, low
gain (G)	29	adjustable PROTEM gain factor; actual gain is 2^G
reduction	30	value of "a" indicates that receiver 4× and 10× gain factors have been removed
integrations	32	PROTEM coded integration time setting
time	45–48	time of measurement in hour-minute format (hhmm)

Table 2–7. Description of the analog PROTEM receiver header record (HDR) data fields (gates).

[TX, transmitter; RX, receiver]

Field (gate)	Contents
0	date of measurement in month-day format (mmdd)
2	time of measurement in hour-minute format (hhmm)
4	TX current (ampere)
5	TX turnoff time (microsecond)
6–7	TX loop side length LX (meter) and LY (meter)
8–9	RX coil position XR (meter) and YR (meter) relative to center of TX loop
10	RX coil moment (turn•square meter)
11	TX number (47 or 57)
22	logger record number for this header record

Table 2–8. Description of the analog PROTEM receiver data record (OPR) data fields (gates).

[TEM, transient electromagnetic; TX, transmitter; RX, receiver]

Field (gate)	Contents
0	logger record number for this data record
1–20	channels 1–20 TEM data (millivolt)
21	TX turnoff time (millisecond)
22	first RX gate time (millisecond)
23	TX current (ampere)
24	TX moment (turn•square meter), may include trailing "/"
25	time of measurement in hour-minute format (hhmm)

The next section of the data page gives the channel number and the voltage induced in the receiver coil divided by the receiver coil moment in units of microvolts per square meter ($\mu V/m^2$). The average of these voltages is computed and expressed as receiver units in millivolts (mV). The standard deviation as a percentage of the average data value is also reported.

The last section of the data page presents the voltages after they have been transformed to apparent resistivity. The print out includes the channel number, the receiver channel time, the square root of the time in seconds ($s^{1/2}$), the late-stage apparent resistivity, the average of the resistivity values, and the percentage standard deviation of the apparent resistivity.

The PRV files from this survey can be found in the data release subdirectory "PRV_DATA" (Fitterman, 2016).

(c) Inversion Summary Files (extension .INV)

The reports generated by the TEM inversion program TEMIXXL have the filename extension .INV. They provide information on the sounding location, the measurement geometry, the model misfit error, the model parameter estimates, the measured resistivity and calculated model response, and usually a resolution matrix.

Misfit error reported by the TEM inversion program (TEMIXXL) is given as percentage root mean square (RMS) misfit for voltage data. The apparent resistivity misfit is approximately two-thirds of this value.

The inversion output files (.INV files) from this survey can be found in the data release subdirectory "INV_DATA" (Fitterman, 2016).

(d) Extracted Data Files (extensions .ROT and .ROZ)

The text files that contain data and models in a form for plotting have the filename extensions .ROT and .ROZ. The .ROT file contains the following information:

1. The sounding name.
2. Tab delimited column headings for the data that follow.
3. Tab delimited time and apparent resistivity data consisting of 6, 9, or 12 columns corresponding to 1, 2, or 3 transmitter repetition frequencies, respectively. Typically, the data are given in order of decreasing repetition frequency corresponding to later time ranges. The contents of the columns are specified in table 2–9.

Table 2–9. Description of plotable data in apparent-resistivity-time files (filename extension .ROT).

[FREQ, base frequency; in FREQn, n refers to the order (first, second, or third) of the transmitter repetition frequencies]

Column[1]	Contents	Description
1	time	time of data point after transmitter turnoff (millisecond)
2	freq1_avg	FREQ1 averaged apparent resistivity (ohm-meter)
3	freq1_std	FREQ1 averaged apparent resistivity standard error
4	freq1_cal	FREQ1 calculated apparent resistivity (ohm-meter)
5	freq2_avg	FREQ2 averaged apparent resistivity (ohm-meter)
6	freq2_std	FREQ2 averaged apparent resistivity standard error
7	freq2_cal	FREQ2 calculated apparent resistivity (ohm-meter)
8	freq3_avg	FREQ3 averaged apparent resistivity (ohm-meter)
9	freq3_std	FREQ3 averaged apparent resistivity standard error
10	freq3_cal	FREQ3 calculated apparent resistivity (ohm-meter)
11	masked	apparent resistivity of a masked data point
12	m_err	standard error of a masked data point

[1]When a sounding has fewer than 3 base frequencies (or sweeps), the unnecessary columns are omitted. The masked and m_err data follow immediately after the last sweep.

The .ROZ files contain the following information:

1. The sounding name.
2. Tab delimited titles for the data that follow: "Depth (m)" and "Resistivity (ohm-m)."
3. Tab delimited data for plotting a resistivity-depth plot. Depths are given as positive values below the surface. The depth sequence will be: 0, z_1, z_1, z_2, z_2, . . . , z_{n-1}, z_{n-1}, z_{n-1} + max(10, 1.2*z_{n-1}). The resistivity sequence will be ρ_1, ρ_1, ρ_2,ρ_2, . . . ρ_{n-1}, ρ_{n-1}, ρ_n, ρ_n.

The extracted data files (.ROT and .ROZ files) from this survey can be found in the data release subdirectory "EXT_DATA" (Fitterman, 2016).

(e) Report Summary Files (extension .RPT)

The sounding report files created by the program TEM_REPORT have the filename extension .RPT and are described further in appendix 4. The report files contain all relevant information for the sounding and its interpretation summarized on one or two pages. The individual report files have been grouped together by field season and are furnished as text files named "TEM_report_*yyyy*.txt" and PDF files named "TEM_report_*yyyy*.pdf," where "*yyyy*" is the field season year. The report files are found in the data release directory "TEMSLV*yyyy*" (Fitterman, 2016).

(f) Inversion Database Files (extension .TX3)

Three database files generated by the inversion program TEMIXXL are included in the data release that accompanies this report. The files are named "*ppppppyy*.TX3," where "*pppppp*" is a character string of up to six characters describing the project ("GRSAND" for this study) and "*yy*" is the field season year. The database files can be found in the data release directory "TEMSLV*yyyy*" where "*yyyy*" is the field season year (Fitterman, 2016).

Appendix 3. Voltage Units and Apparent Resistivity

Measured electromagnetic transients can be reported in two different ways: as the voltage recorded in the receiver itself or as the voltage at the receiver coil normalized by the receiver-coil moment (number of coil turns times the coil area). The voltage at the receiver coil (V_{coil}) can be determined using Faraday's Law:

$$V_{coil} = -M_{Rx}\frac{d\mathbf{B}\cdot\hat{\mathbf{n}}}{dt} = -M_{Rx}\frac{dB}{dt}, \tag{3–1}$$

where

$\mathbf{B}$ is the magnetic induction in webers per square meter (Wb/m^2),
$\hat{\mathbf{n}}$ is the unit normal to the receiver coil (assumed to be vertical),
t is time, and
M_{Rx} is the receiver-coil moment.

Rearranging equation 3–1 gives the equation

$$\frac{V_{coil}}{M_{Rx}} = -\frac{dB}{dt}. \tag{3–2}$$

This representation of the data is convenient for comparison against background electromagnetic noise levels, which are typically 0.1–1 nanovolt per square meter (nV/m^2) (Fitterman, 1989). All units are International System (SI).

For the PROTEM receivers used in this study, the voltage at the coil (V_{coil}) and the voltage recorded at the receiver (V_{Rx}) are related by

$$V_{coil}[\mathrm{nV}] = \frac{10^{-6}V_{Rx}[\mathrm{mV}]}{52.1\cdot 2^{G}}, \tag{3–3}$$

where G is the receiver gain setting (see table 2–2 or 2–6) and the factor 52.1 accounts for additional fixed receiver gain. Units are shown in square brackets (nV, nanovolt; mV, millivolt). The magnitude of the time derivative of the magnetic induction is then calculated with the equation

$$\frac{dB}{dt}[\mathrm{nV/m^2}] = \frac{V_{coil}[\mathrm{nV}]}{M_{Rx}[\mathrm{m^2}]} = \frac{10^{-6}V_{Rx}[\mathrm{mV}]}{52.1\cdot 2^{G}M_{Rx}[\mathrm{m^2}]}. \tag{3–4}$$

Units are shown in square brackets (m^2, square meter).

The late-stage apparent resistivity (ρ_a^{LS}) (Kaufman and Keller, 1983; Fitterman and Labson, 2005) is computed from the voltage induced in the receiver coil (V_{coil}) by the equation

$$\rho_a^{LS} = \frac{\mu_0}{4\pi t}\left[\frac{2\mu_0 L^2 M_{Rx} I_{Tx}}{5tV_{coil}}\right]^{2/3}, \tag{3–5}$$

where

t is the time after current turn off,
L is the square transmitter loop side length,
I_{Tx} is the transmitter current, and
μ_0 is the magnetic permeability of free space (H/m, henry per meter), equal to = $4\pi\cdot 10^{-7}$ [H/m].

Recasting equation 3–5 into typical field units and incorporating the PROTEM gain constants

$$\rho_a^{LS}[\text{ohm-m}] = \frac{10^{-4}}{t[ms]}\left\{\frac{0.16\cdot\pi\cdot 52.1\cdot 2^{G}L^2[\mathrm{m^2}]M_{Rx}[\mathrm{m^2}]I_{Tx}[\mathrm{A}]}{t[\mathrm{ms}]V_{Rx}[\mathrm{mV}]}\right\}^{2/3} \tag{3–6}$$

and

$$\rho_a^{LS}[\text{ohm-m}] = \frac{0.1}{t[\mu s]}\left\{\frac{160\cdot\pi\cdot 52.1\cdot 2^{G}L^2[\mathrm{m^2}]M_{Rx}[\mathrm{m^2}]I_{Tx}[\mathrm{A}]}{t[\mu s]V_{Rx}[\mathrm{mV}]}\right\}^{2/3}. \tag{3–7}$$

Units are shown in square brackets (ohm-m, ohm-meter; ms, millisecond; A, ampere; μs, microsecond).

Appendix 4. Description of Transient Electromagnetic (TEM) Sounding Report Files and Plots

Transient electromagnetic (TEM) sounding reports and plots are provided in directories, described here, that can be found in the data release by Fitterman (2016) that accompanies this data series.

There is one subdirectory for each field season with the name "TEMSLV*yyyy*" where *yyyy* is the year the data were collected. The contents of each field season folder are as follows:

4. Inversion results for all soundings as a portable document format (PDF) file (TEM_report_*yyyy*.pdf)
5. Inversion results for all soundings as a text file (TEM_report_*yyyy*.txt)
6. TEM resistivity-time and resistivity-depth plots as PDF files (TEM_plots_*yyyy*.pdf)
7. Raw data files subdirectory (RAW_DATA)
8. Averaged data report files subdirectory (PRV_DATA)
9. Averaged data files subdirectory (AVG_DATA)
10. Inversion output files subdirectory (INV_DATA)
11. Extracted data files subdirectory (EXT_DATA)
12. TEMIXXL database file (GRSAND*yy*.TX3)

The reports and plots found in the online directories summarize the TEM data and inversion results for each sounding location. Some of the soundings have an alternative interpretation; names for those soundings include the letter "L" after the sounding identifier followed by a number indicating the number of layers in the alternate model.

Most of the entries in the reports are self-explanatory; a few that may not be are described in more detail below.

Misfit Error

The resistivity-depth models determined by inversion are usually not unique; that is, there is uncertainty in the estimated model parameters caused by observation and parameterization errors. Observational errors are caused by electromagnetic and instrumental noise. Parameterization errors are attributable to naturally occurring variations in geology that are not describable by the one-dimensional (layered earth) model used for the inversion. The misfit error gives an estimate of how well the inversion agrees with the observed data

Resolution Matrix

Another issue in the inversion is the resolution of the model parameters. To understand model resolution, assume that there is an actual set of model parameters that we can only view through a set of glasses. If the glasses give a good image of the actual parameters, then the resolution is good. If, on the other hand, the glasses distort the viewing of the actual parameters, then the resolution is poor. In the inversion report, the diagonal members of the inversion resolution matrix are given to the right of the model parameters. The column marked "RR" is the resolution of the layer resistivities, while the column marked "RT" is the resolution of the layer thicknesses. Occasionally in the report, the resolution values are described using qualitative terms based on a somewhat arbitrary scale: excellent (0.95–1.00), very good (0.80–0.95), good (0.50–0.80), poor (0.25–0.50), and very poor (0.00–0.25).

Transient Electromagnetic (TEM) System Designation

This coding specifies the type of PROTEM receiver used. A digital PROTEM-D receiver is designated by "EM-58." An analog PROTEM receiver is marked as "EM-x7." These are the labels output by the Geonics Limited receivers in the raw data files; they are preserved in the first line of the averaged data files.

Dataset Frequency Code

Six dataset codes are used to identify the combination of transmitter type (EM-47 or EM-57) and frequency, or repetition rate, used (see table 4–1). Transmitter type can also be determined from the PROTEM and PROTEM-D raw and averaged data files by looking at data field 11 of the header record (HDR) (see table 2–3). An indirect and not completely reliable indication of the transmitter used is the transmitter current: the maximum current for the EM-47 transmitter is about 3.0 amperes (A), whereas the maximum current for the EM-57 transmitter is about 25 A. Also, a higher bandwidth receiver coil is required for the 285-hertz repetition rate used for EM-47 data. The high-bandwidth Geonics Limited receiver coil designed for use with the EM-47 transmitter has a moment of 31.4 square meters (m^2), whereas the EM-57 transmitter, which operates at lower repetition rates (frequencies), usually uses a receiver coil with a moment of 100 m^2 or 200 m^2.

Table 4–1. Dataset frequency codes used in report files.

Transmitter	Frequency (hertz)	Code
EM-47	285	uh
	75	vh
	30	hi
EM-57	30	HI
	7.5	MD
	3	LO

Publishing support provided by:
Denver Publishing Service Center, Denver, Colorado

For more information concerning this publication, contact:

Program Coordinator, National Cooperative Geologic Mapping Program
12201 Sunrise Valley Drive, Mail Stop 908
Reston, VA 20192
(703) 648-6053

Or visit the Geosciences and Environmental Change Science Center Web site at:
https://ncgmp.usgs.gov/

This publication is available online at:
https:/doi.org/10.3133/ds1043

ISSN 2327-638X (online)
https://doi.org/10.3133/ds1043